

COMPUTER MODELING OF BLOWBACK OIL CONSUMPTION IN
INTERNAL COMBUSTION ENGINES

A THESIS SUBMITTED TO
THE GRADUATE SCHOOL OF NATURAL AND APPLIED SCIENCES
OF
MIDDLE EAST TECHNICAL UNIVERSITY

BY

EGEMEN BİLGE

IN PARTIAL FULFILLMENT OF THE REQUIREMENTS
FOR
THE DEGREE OF MASTER OF SCIENCE
IN
MECHANICAL ENGINEERING

SEPTEMBER 2009

Approval of the thesis:

**COMPUTER MODELING OF BLOWBACK OIL CONSUMPTION IN
INTERNAL COMBUSTION ENGINES**

submitted by **EGEMEN BİLGE**, in partial fulfillment of the requirements for the degree of **Master of Science in Mechanical Engineering Department, Middle East Technical University** by,

Prof. Dr. Canan Özgen
Dean, **Graduate School of Natural and Applied Sciences**

Prof. Dr. Süha Oral
Head of Department, **Mechanical Engineering**

Prof. Dr. Zafer Dursunkaya
Supervisor, **Mechanical Engineering Dept., METU**

Examining Committee Members:

Instr. Dr. Tahsin Çetinkaya
Mechanical Engineering Dept., METU

Prof. Dr. Zafer Dursunkaya
Mechanical Engineering Dept., METU

Asst. Prof. Dr. Cüneyt Sert
Mechanical Engineering Dept., METU

Dr. Ahmet Yozgatlıgil
Mechanical Engineering Dept., METU

Dr. H. Tuğrul Tınaztepe
Roketsan Missiles Industries Inc.

Date: 09.09.2009

I hereby declare that all information in this document has been obtained and presented in accordance with academic rules and ethical conduct. I also declare that, as required by these rules and conduct, I have fully cited and referenced all material and results that are not original to this work.

Name, Last name : Egemen Bilge

Signature :

ABSTRACT

COMPUTER MODELING OF BLOWBACK OIL CONSUMPTION IN INTERNAL COMBUSTION ENGINES

Bilge, Egemen

M. Sc., Department of Mechanical Engineering

Supervisor: Prof. Dr. Zafer Dursunkaya

September 2009, 71 pages

Environmental pollution is an important problem of our world. Governments are aware of this problem and emission regulations are continuously improved. One of the strictest regulations is about unburned and burned hydrocarbon emissions. In internal combustion engines the origin of the burned and unburned hydrocarbons is fuel and engine oil. As a result of the sanctions and the necessity of improved combustion performance of the engine, manufacturers work on manufacturing technology and engine tribology. With the improvement of these areas oil loss from internal combustion engine is reduced. Engine oil consumption mechanisms are specific research areas in the internal combustion engine development. Oil consumption occurs via to two main routes: “Valve train” and “in cylinder components”. In cylinder components have three sub mechanisms: evaporation, ring scraping and blowback. In this thesis, blowback oil loss mechanism is studied.

2D flow model of piston-cylinder mechanism is developed in Fluent. Land pressures and ring end gap flow data are taken from this model. An iterative computer program is developed to calculate backflow oil consumption. In this program, an empirical entrainment correlation compiled from literature is used. The calculated oil consumption values match with the range of the values in the literature.

Keywords: Oil consumption, Internal combustion engines, Oil entrainment, Oil blowback.

ÖZ

İÇTEN YANMALI MOTORLARDAKİ GERİ AKIŞLA YAĞ KAYBININ BİLGİSAYAR MODELLEMESİ

Bilge, Egemen

Yüksek Lisans, Makina Mühendisliği Bölümü

Tez Yöneticisi: Prof. Dr. Zafer Dursunkaya

Eylül 2009, 71 sayfa

Çevre kirliliği dünyamızın önemli bir problemidir. Hükümetler bu problemin farkındadırlar ve emisyon ile ilgili yasaları gittikçe daha katı hale getirmektedirler. En katı yasalardan biri de yanmış ve yanmamış hidrokarbon emisyonları ile ilgilidir. İçten yanmalı motorlarda yanmış ve yanmamış hidrokarbonların kaynağı yakıt ve motor yağıdır. Yasal yaptırımlar ve motor performansındaki ilerleme ihtiyacının bir sonucu olarak üreticiler üretim teknikleri ve motor tribolojisi üzerine çalışmaktadırlar. Bu alanlardaki gelişimle birlikte içten yanmalı motorlardaki yağ kaybı da azalmaktadır. Motor yağ kaybı mekanizması içten yanmalı motorların gelişiminde önemli bir araştırma alanıdır. Yağ kaybı iki yolla oluşmaktadır: “sübağ gurubu” ve “silindir içi parçalar”. Silindir içi parçalar da üç alt mekanizmayla yağ kaybına neden olmaktadır: buharlaşma, sekmanın yağı sıyırması ve yağın gaz ile geri akışı. Bu araştırmada, bu mekanizmalardan yalnızca yağ geri akışı

incelenmektedir. Piston-silindir mekanizmasının iki boyutlu gaz akış modeli Fluent programı kullanılarak geliştirilmiştir. Sekmanlar arası hacimlerdeki basınçlar ve sekman uç boşluklarındaki akış verileri bu modelden alınmıştır. Yağ geri akışının hesaplanabilmesi için bir bilgisayar kodu geliştirilmiştir. Bu programda literatürden alınan deneysel sıvı kopma denklemleri kullanılmıştır. Hesaplanan yağ kaybı değerleri literatür değerleri ile benzerlik göstermiştir.

Anahtar Kelimeler: Yağ kaybı, İçten yanmalı motorlar, Yağ koparma, Yağ geri akışı.

To Bahar and Defne

ACKNOWLEDGEMENTS

I would like to express my gratitude to Prof. Dr. Zafer Dursunkaya for his supervision, continuous support and guidance at every step of this thesis.

I am grateful to Suzan Koç and other colleagues at ROKETSAN for their patience and encouragement. I am thankful to my colleagues Murat Akkuş, Funda Eroğul, Satılmış İnal and M. Yusuf Yılmaz for their devoted study to compensate my absence in the company.

I would also like to thank to my colleagues and friends Bora Kalpakli and Onur Baş for their crucial advises, friendship and Fluent assistance.

I owe a special thank to my family and in-laws for their precious support and encouragement.

Special thanks to my beautiful daughter Defne, for her waking me up every morning at 6 to pull for study (!); but the most important of all, for all the happiness and joy she has brought to my life since the day she was born.

Finally, I want to express my feelings of love to my wife, Bahar, since without her patience and support this work would not be completed.

TABLE OF CONTENTS

ABSTRACT	iv
ÖZ	vi
ACKNOWLEDGEMENTS.....	ix
TABLE OF CONTENTS	x
LIST OF TABLES.....	xii
LIST OF FIGURES	xiii
LIST OF SYMBOLS.....	xv
CHAPTERS	
1 INTRODUCTION	1
1.1 Fundamentals of Oil Blowback	2
1.1.1 Oil flow route.....	3
1.1.2 Oil film thickness variation.....	5
1.1.3 Entrainment	6
1.2 Scope of the Current Study.....	10
2 MODELING OF THE PROBLEM	11
2.1 Modeling of Piston and Cylinder.....	11
2.2 Modeling of Gas Flow	16
2.3 Oil Gas Interface Velocity	19
2.4 Oil Flow Model.....	21
2.4.1 Entrainment rate calculation.....	21
2.4.2 Conservation of mass for oil.....	24

3	RESULTS AND DISCUSSION.....	27
3.1	Gas Flow Analysis Results.....	27
3.2	Oil Flow Analysis Results.....	48
4	CONCLUSIONS.....	61
	REFERENCES.....	63
	APPENDIX A. OIL GAS INTERFACE VELOCITY CALCULATION.....	66

LIST OF TABLES

TABLES

Table 2.1 Dimensions of the modeled heavy duty diesel engine	13
Table 2.2 Physical properties of fluids	21

LIST OF FIGURES

FIGURES

Figure 1.1 Oil blowback mechanism	3
Figure 1.2 Pressure variation during combustion	3
Figure 1.3 Oil and air flow routes [3]	4
Figure 1.4 Piston and land passages	4
Figure 1.5 Gas and oil passage area.....	5
Figure 1.6 Inception criteria	7
Figure 2.1 Schematic diagram of ring package	12
Figure 2.2 Piston-cylinder assembly.....	12
Figure 2.3 3D surface geometry of gas between piston and cylinder (to scale).....	14
Figure 2.4 2D geometry of volumes between piston and cylinder and gas flow path (to scale).....	14
Figure 2.5 Modified 2D geometry (to scale)	16
Figure 2.6 2D mesh (11065 cells, 23094 faces and 12075 nodes) (to scale).....	18
Figure 2.7 Representation of gas flow model [14]	20
Figure 2.8 Oil entrainment mechanism	22
Figure 2.9 Ring end gap and oil film.....	24
Figure 3.1 Land volume pressures at 2100 rpm, full load (comparison with [14]).	28
Figure 3.2 Land volume pressures at 500 μm top ring end gap.....	29
Figure 3.3 Land volume pressures at different top ring end gaps	30
Figure 3.4 2 nd land peak pressures at different top ring end gaps.....	32
Figure 3.5 3 rd land peak pressures at different top ring end gaps.....	34
Figure 3.6 Land volume peak pressures at full and 50% load.....	35
Figure 3.7 Land volume peak pressures at different engine loads	37

Figure 3.8 Blowby (at different engine loads).....	38
Figure 3.9 Efect of speed on blowby and top ring axial motion, at full load [15]...39	39
Figure 3.10 Mach contours at maximum combustion chamber pressure	41
Figure 3.11 Mach contours at maximum combustion chamber pressure	44
Figure 3.12 Mach contours at maximum 2nd land pressure.....	45
Figure 3.13 Mach contours at maximum 1st land pressure	48
Figure 3.14 Backflow oil transfer to combustion chamber at different oil film thickness	49
Figure 3.15 Backflow oil transfer to combustion chamber at different engine speeds and loads	51
Figure 3.16 Backflow oil transfer to combustion chamber at different engine loads and speeds.....	53
Figure 3.17 Backflow oil transfer to combustion chamber at different engine loads and oil thicknesses	55
Figure 3.18 Backflow oil transfer to combustion chamber for different oil viscosities at 2100 rpm full load.....	58
Figure 3.19 Backflow oil transfer to combustion chamber for different oil viscosities at 2100 rpm full load.....	59
Figure 3.20 Oil consumption for different physical properties and dimensions	60

LIST OF SYMBOLS

A	Ring end gap cross sectional area (m ²)
b ₁	Integration constant
D	Diameter (m)
D _h	Hydraulic diameter (m)
E	Entrainment fraction
h	Radial distance between gas core and cylinder (m)
H	Distance of groove top from the piston crown (m)
J	Volumetric flux (m ³ /s)
m	Mass (kg)
P	Pressure (bar)
Re	Reynolds number
R _g	Ring end gap (m)
R _r	Distance between piston and cylinder (m)
R _t	Ring thickness (m)
t	Oil film thickness (m)
t _g	Ring groove thickness (m)
V	Velocity (m/s)
We	Weber number
y	Radial distance from air-oil interface (m)
y [*]	Radial distance from cylinder wall (m)
z	Axial distance from the beginning of the ring end gap (m)

Other Symbols:

\forall	Volume (m^3)
ρ	Density (kg/m^3)
σ	Surface tension (N/m)
μ	Dynamic viscosity ($\text{N}\cdot\text{s}/\text{m}^2$)
$\dot{\epsilon}$	Entrainment rate (kg/s)
δ	Velocity profile displacement thickness
ζ	Axial dimensionless distance from the beginning of the ring end gap
ν	Kinematic viscosity (m^2/s)

Subscripts:

gas	Gas
oil	Oil
max	Maximum
ent	Entrainment
f	Liquid
g	Gas

CHAPTER 1

INTRODUCTION

One of the crucial problems of our world is environmental pollution. Governments attract public and businessmen's attention to environmental pollution by keeping strict environmental regulations. Because of the strict regulations, particularly automobile manufacturers work on decreasing unburned and burned hydrocarbon emissions. With better understanding of combustion phenomenon, oil is becoming a major contributor to burned and unburned hydrocarbon emission. Besides the hydrocarbon emissions, engine performance and engine life is also affected by oil consumption. There are two main mechanisms of the oil consumption. First of all, oil consumption occurs due to the valve train, which accounts for approximately 15-25% of total oil loss [1]. Rocker arms, valve springs, push rods, lifters and cam mechanism are the components of the valve train. Valve train oil consumption occurs especially through the valve cover during the lubrication and cooling operation. The remaining 75-85% of oil loss occurs due to in cylinder components [1]. Oil loss due to in cylinder components has three sub mechanisms. First mechanism is the evaporation. During the combustion operation, oil on the piston cylinder surface evaporates from the cylinder walls accounting to 5-10% of total oil loss [2]. The second oil loss mechanism is the scraping of oil by the top compression ring. This mechanism starts at the bottom dead center (BDC) of the piston. During the upward motion of the piston, top compression ring scrapes the oil to the combustion chamber and following the combustion, during the expansion;

oil spreads over the combusted air. Finally, during the exhaust the spread oil is moved out by the exhaust. The final oil consumption mechanism is the blowback oil consumption mechanism which is examined in the current study and explained in following paragraphs. Exact percentages of the scraping and blowback oil loss are not available in the literature.

1.1 Fundamentals of Oil Blowback

Diesel engines studied during this thesis are four stroke. Cross-section of piston and cylinder assembly can be seen in Figure 1.1. The space between piston and cylinder is divided into two volumes with three rings. These inter ring volumes are called the 2nd and 3rd land (Figure 1.1). The variation of pressure in the combustion chamber can be seen in Figure 1.2. This pressure curve can be divided into four strokes according to the piston and valve positions. These strokes are the intake, the compression, the expansion and the exhaust. During the compression process, combustion chamber pressure increases quickly, but 2nd and 3rd land pressures cannot increase as quickly as the combustion chamber (Figure 1.2). Therefore; some of the combustion gases flow to the crankcase, a phenomenon called blowby. During the expansion stroke, the opposite happens and the combustion chamber pressure decreases quickly but the land pressures cannot. Therefore gases flow from the lands to the combustion chamber, which is called blowback (Figure 1.1). Air blowback causes blowback of oil also. To understand oil blowback mechanism there are three sub research areas in the literature. One of the research area is about flow route of oil and air between combustion chamber and crank case. Second research area is about oil film thicknesses between crank case and combustion chamber. the final research area is about the entrainment of oil into flowing gas.

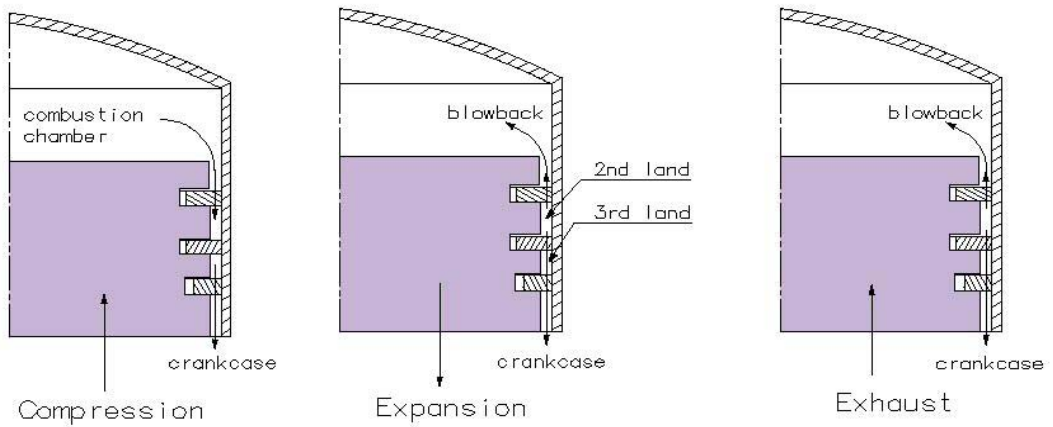


Figure 1.1 Oil blowback mechanism

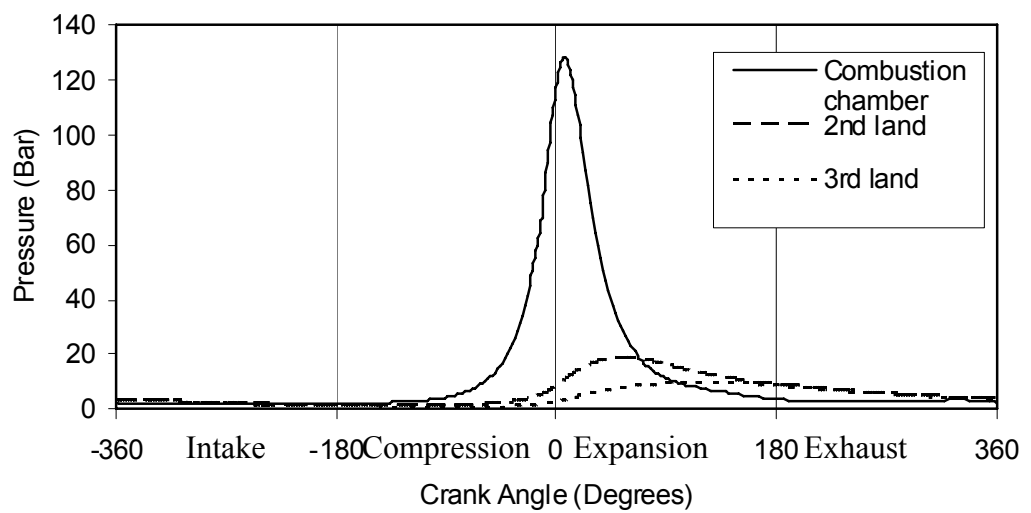


Figure 1.2 Pressure variation during combustion

1.1.1 Oil flow route

Nakashima et al. [3] have studied the flow of oil and air around the piston on a modified engine with glass cylinder. Two routes of oil flow were observed: a major route and a minor route. Major route, where most of the oil flows, includes oil ring groove and the land passages (denoted by thick arrows in Figure 1.3). Oil follows

the ring end gap and land passages (Figure 1.4) to flow into the combustion chamber. Detailed view of oil ring end gap area is given in Figure 1.5. Minor route of oil flow occurs due to the thermal and elastic deformations leading to clearances between piston and cylinder. Oil flows through the peripheral surface of the piston (denotes by thin arrows in Fig. 1.3).

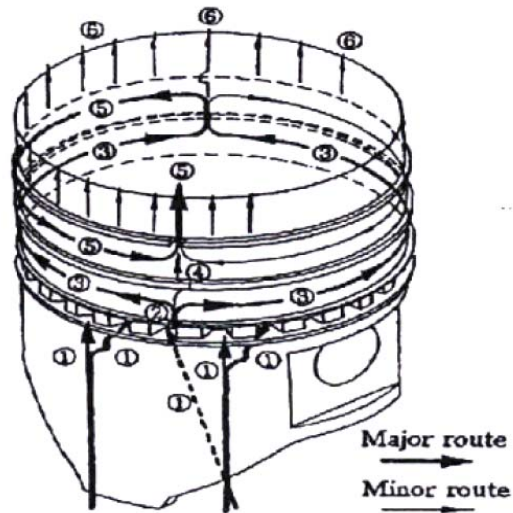


Figure 1.3 Oil and air flow routes [3]

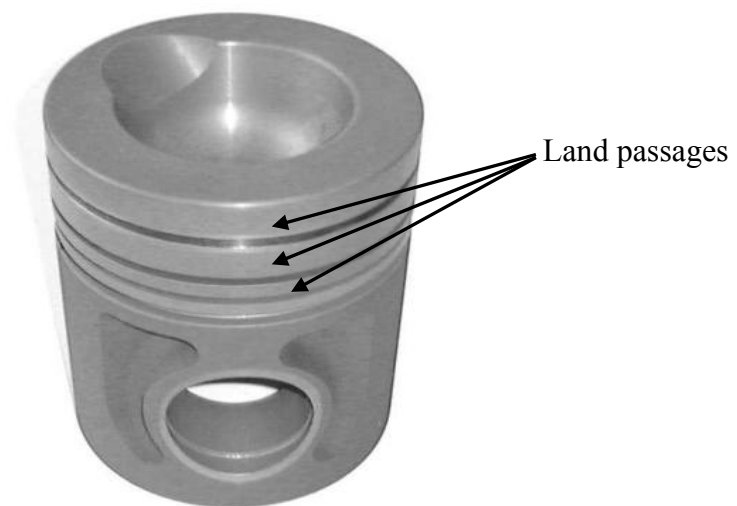


Figure 1.4 Piston and land passages

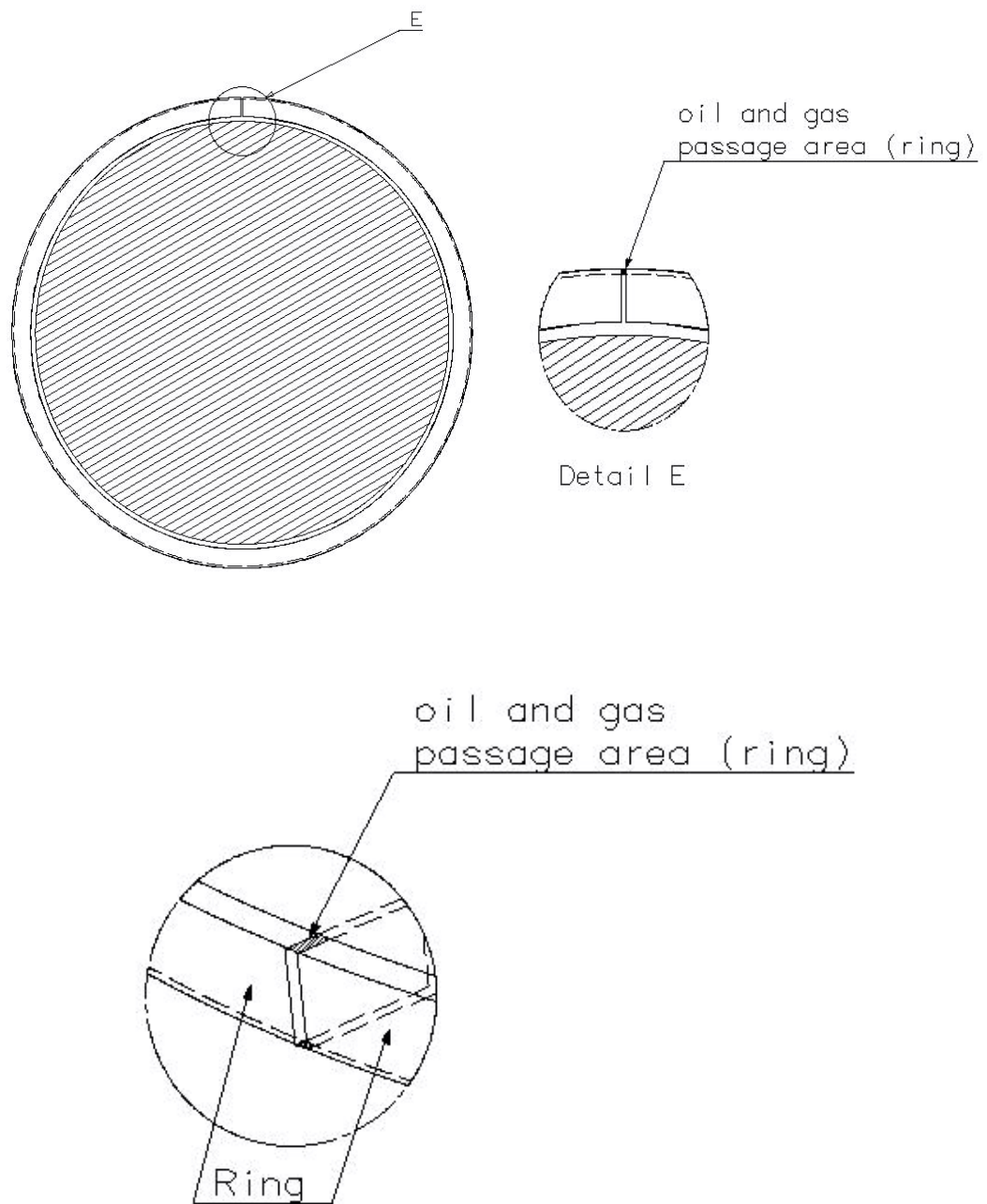


Figure 1.5 Gas and oil passage area

1.1.2 Oil film thickness variation

Wong and Hoult [4] constructed an experimental setup to measure oil consumption and oil thickness in two IDI (indirect injection) diesel engines. Radioactive tracer and laser fluorescence diagnostics were used to measure oil consumption and oil

thickness, respectively. The results show that the oil film thickness change from the combustion chamber to the crank case. Different oil, different engine speed and different oil control ring effects were also studied. Besides, piston skirt oil pumping mechanism and rotation of the ring were also examined.

1.1.3 Entrainment

During the two phase flow of gas and liquid, gas flow tries to tear the liquid from the interface. Fluid physical properties and flow rates affect the amount of liquid droplets consumed into the gas flow, which is called entrainment. Since 1950, researchers have studied the entrainment phenomenon and experimental setups were constructed, numerous of tests were done and several empirical correlations were found. In the following paragraphs, some entrainment studies are explained briefly.

Woodmansee and Hanratty [5] constructed a parallel air flow experimental setup to examine critical conditions of liquid entrainment. It was found that the liquid flow rate does not affect the entrainment rate for thick liquid films. But starting of the entrainment is affected by gas velocity. On the contrary, the entrainment rate is sensitive to liquid flow rate change for very thin liquid films. However; it is insensitive to the change of gas velocity. In both cases, viscosity was determined to have no impact on entrainment.

Hughmark [6] developed a computer program to predict film thickness and entrainment rate of liquid by using upward annular and dispersed flow experimental data. Input file of the program consists of the mass flow rates of the gas and liquid, tube diameter and physical properties of the fluid.

Ishii and Grolmes [7] tried to explore starting point of droplet entrainment in concurrent two phase flow. In their model, film Reynolds number must be higher

than 160. Besides, in higher film Reynolds number, there is a critical gas velocity below which the entrainment is not observed (Fig. 1.6).

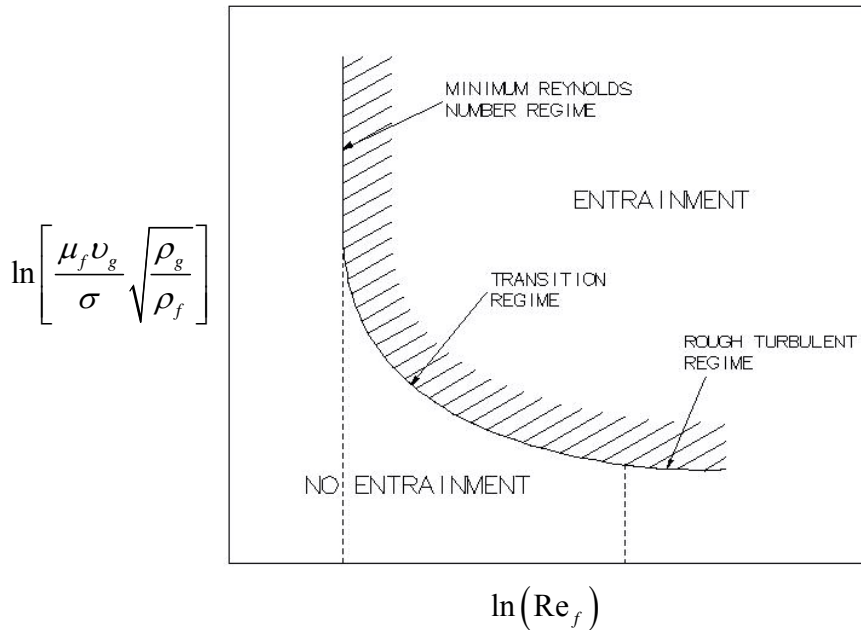


Figure 1.6 Inception criteria

Ishii and Mishima [8] derived an equilibrium entrainment correlation for annular two phase flow. Annular two phase flow is divided into two regions according to the entrainment. First region is the entrance region and the second region is equilibrium region. The derived equilibrium entrainment correlation is related with an effective Weber number and film Reynolds number. In addition, the effect of entrance region on entrainment was examined.

Kataoka et al. [9] worked on deriving an entrainment correlation which covers both entrance and equilibrium regions. Entrainment rate correlation was developed with the help of Weber number, liquid Reynolds number and dimensionless distance from the inlet. The dimensionless distance from inlet was also derived in terms of Weber number, liquid Reynolds number, and hydraulic diameter. In this study,

entrance region effects on entrainment rate and deposition rates were also examined separately.

Okawa et al. [10] derived an entrainment rate correlation, which is applied to 17 sets of experimental data. Entrainment of droplets is calculated using a dimensionless number, which is the ratio of the interfacial shear force to the retaining force of surface tension. Derived entrainment rate correlation needs two experimental coefficients which are mass transfer coefficient of deposition and entrainment.

Okawa and Kataoka [11] used previously obtained air-water experimental data and derived a liquid mass transfer rate correlation, including entrainment and deposition rates for vertical upward annular flow. The derived entrainment rate correlation is based on the ratio of interfacial shear force to the surface tension force acting on the phase interface. In the derivation of the deposition rate correlation, superficial gas velocity is taken as the most important parameter for low droplet concentration. On the other hand, droplet concentration is important in high droplet concentration gas flow.

Sawant et al. [12] intended to derive a new entrainment rate correlation which can be applied to high pressure and high speed flows. In this study, a new modified Weber number is derived and its pressure sensitivity was improved. Entrainment rate is primarily dependent to modified Weber number and film Reynolds number. Up to a value of Weber number, entrainment rate is proportional to modified Weber number and does not depend on film Reynolds number. From this modified Weber number limit to another higher limit of the modified Weber number, entrainment rate is related with both modified Weber number and film Reynolds number. If modified Weber number value is higher than these limits, then entrainment rate only depends on film Reynolds number. In this procedure, in order to use the new entrainment rate correlation and to predict an important coefficient, an initial prediction for the maximum possible entrainment rate is needed.

İçöz [13] constructed an experimental setup represented cylinder piston ring assembly in Cartesian geometry to examine oil film thickness effect on oil accumulation in the 2nd land volume. Mixture of oil gas is obtained after a single piston stroke and oil content is analyzed by gas chromatograph.

Karkaç [14] constructed zero dimensional model of piston and cylinder assembly to determine land pressures, ring end gap mass flow rates and gas velocities through the ring end gap. In his study, three volumes represent combustion chamber, 2nd and 3rd lands. These lands are connected with ring end gaps. Flow through the ring end gaps are simulated by one-dimensional orifice flow. Besides, choked flow assumption is used for the ring end gap flow. By using conservation of mass, land pressures are predicted.

Keribar et al. [15] developed a model to predict ring pack performance and this model includes ring-liner hydrodynamic and boundary lubrication, friction; ring axial, radial and twist dynamics; inter-ring gas dynamics and blowby.

Miyachika et al. [16] measured combustion chamber pressure, second land pressure and oil consumption of four stroke gasoline engine at different engine speeds. 2nd land pressure and oil consumption relation also tried to investigated. They used sulfur as a tracer to determine oil consumption.

Lizumi and Koyama [17] worked on a four stroke 6 cylinder in-line, water-cooled, direct injection, naturally-aspirated diesel engine to determine oil consumption values. In this research, S-trace method is used to determine oil consumption first time in the literature. They found that S-trace method is faster than weight method in determining oil consumption. Oil consumption is also measured in transient operation.

1.2 Scope of the Current Study

In this study, it is proposed to constitute a computer model of cylinder piston ring assembly. By using the computer model, 2nd and 3rd land volume pressures are obtained given combustion chamber pressure variation for different engine speed and load conditions. Land volume pressures change with the change of top ring end gap. Mass flow rates and velocities through ring end gaps are also taken from the computer model. From these data, blowby and blowback values are calculated. In addition, an oil entrainment model is constructed to analyze oil consumption of the engines. Land pressure peak values and pressure curves are compared with the literature. Blowby and oil consumption results are compared with the values available in the literature. Details of the gas and oil modeling and the results are given in the following chapters.

CHAPTER 2

MODELING OF THE PROBLEM

Oil consumption mechanism in internal combustion engines is a complex phenomenon to understand and to model in a computer. In the former chapter, a brief explanation of oil consumption mechanisms in internal combustion engines was given. In this study, blowback oil consumption mechanism with constant oil thickness throughout the cylinder surface is examined by developing a computer model. Explanation about modeling methodology and parts of the modeling of the problem are given below. To develop a computer model of the oil consumption mechanism in the internal combustion engine, initially a model of the gas flow between piston and cylinder must be generated. In the current study, air flow is modeled as 2D, which is different from the previous studies [14]. After modeling the air flow, air-oil interface velocity is calculated by an iterative computer code. Finally, oil entrainment and oil mass conservation model are developed.

2.1 Modeling of Piston and Cylinder

In the real case, piston and cylinder have 3D cylindrical geometry. But to analyze the gas flow, it is enough to model gas between piston and cylinder. Piston and cylinder properties are listed in Table 2.1. As it can be seen on Table 2.1, Figure 2.1 and Figure 2.2, difference between bore and land diameters are too small.

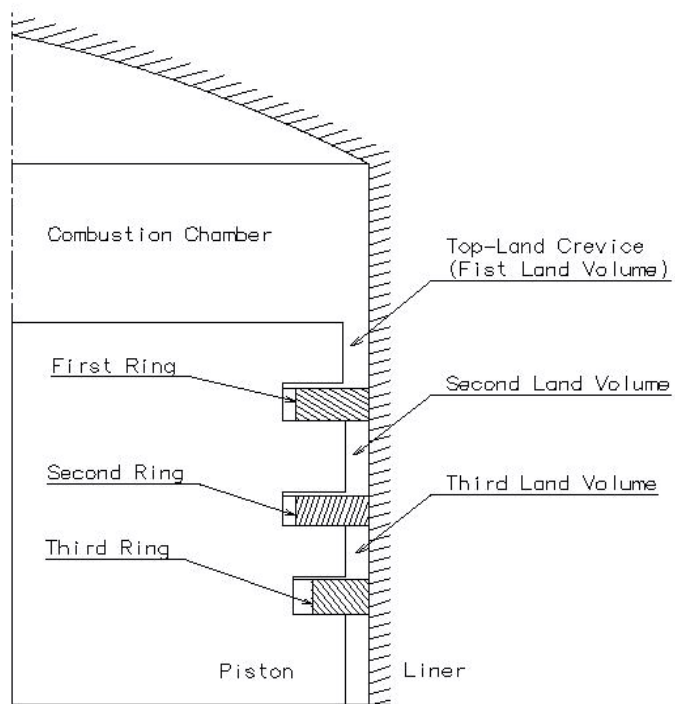


Figure 2.1 Schematic diagram of ring package

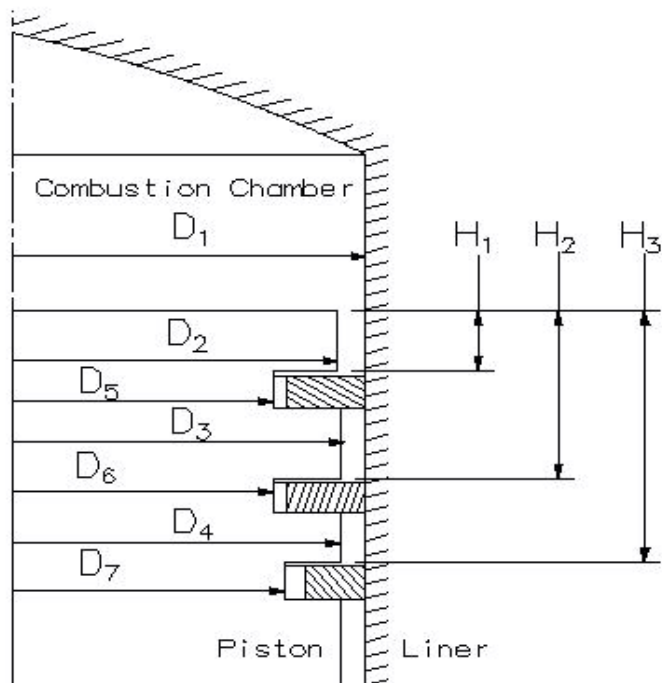


Figure 2.2 Piston-cylinder assembly

Table 2.1 Dimensions of the modeled typical heavy duty diesel engine

Piston Dimensions		
Bore Diameter	D ₁	125 mm
Stroke		140 mm
Number of Rings		3
1 st Land Diameter	D ₂	124 mm
2 nd Land Diameter	D ₃	124.44 mm
3 rd Land Diameter	D ₄	124.44 mm
1 st Groove Diameter	D ₅	112.27 mm
2 nd Groove Diameter	D ₆	112.27 mm
3 rd Groove Diameter	D ₇	114.36 mm
Ring End Gaps		0.5 mm
1 st Ring Groove Thickness	t _{g1}	3.5 mm
2 nd Ring Groove Thickness	t _{g2}	3.2 mm
3 rd Ring Groove Thickness	t _{g3}	3.5 mm
Distance of Groove Top From The Piston Crown 1	H ₁	5.7 mm
Distance of Groove Top From The Piston Crown 2	H ₂	16 mm
Distance of Groove Top From The Piston Crown 3	H ₃	24 mm
Ring Dimensions		
Thickness of 1 st Ring		3 mm
Thickness of 2 nd Ring		2.8 mm
Thickness of 3 rd Ring		3.2 mm
Width of 1 st Ring		5.1 mm
Width of 2 nd Ring		5.1 mm
Width of 3 rd Ring		3.4 mm

First of all, the 3D geometry of the spacing between piston and cylinder is modeled. However; generating mesh and analyzing flow in this thin volume cause problems, which are explained in the following section. Therefore, 3D geometry is modeled as

a 3D surface (Fig. 2.3). To modify this 3D surface to a 2D surface, geometry is cut from combustion chamber to the crank case and lied out on a Cartesian surface (Fig. 2.4). After cutting operation, cut lines are matched by using the periodic boundary condition option in Fluent. After that, these cut lines represent the same line and fluid can flow from one side to the other side of the line as in the real case.

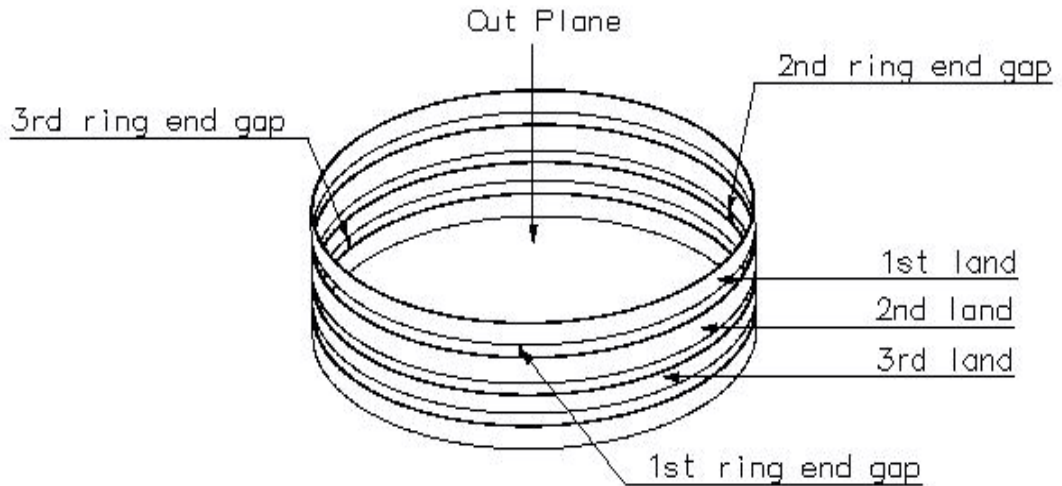


Figure 2.3 3D surface geometry of gas between piston and cylinder (to scale)

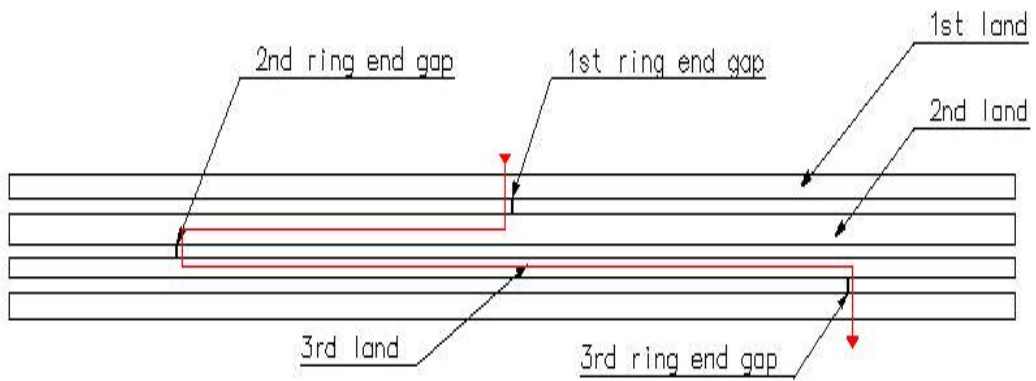


Figure 2.4 2D geometry of volumes between piston and cylinder and gas flow path (to scale)

From Table 2.1 there is a small difference between 1st, 2nd and 3rd land diameters. This difference causes volumetric differences also. If 3D geometry is simplified to the 2D geometry, because the geometry is drawn according to the bore diameter, some volume is lost. Actual 3D and 2D land volume calculations are given below.

Actual volume of 1st land (\forall_1):

$$\forall_1 = \frac{\pi(D_1^2 - D_2^2)}{4} h_1 \quad (2.1)$$

Actual volume of 2nd land (\forall_2):

$$\forall_2 = \frac{\pi(D_1^2 - D_3^2)}{4} (h_2 - h_1 - t_{g1}) \quad (2.2)$$

Actual volume of 3rd land (\forall_3):

$$\forall_3 = \frac{\pi(D_1^2 - D_4^2)}{4} (h_3 - h_2 - t_{g2}) \quad (2.3)$$

Volume calculations of the lands in 2D geometry:

In Fluent analysis, if there is 2D geometry, the program takes the surfaces as a volume with a surface area times one meter deep volume.

1st land Volume (\forall_1')

$$\forall_1' = \pi D_1 h_1 (1m) \quad (2.4)$$

2nd land Volume (\forall_2')

$$\forall_2' = \pi D_1 (h_2 - h_1 - t_{g1}) (1m) \quad (2.5)$$

3rd land Volume (\forall_3')

$$\forall_3' = \pi D_1 (h_3 - h_2 - t_{g2}) (1m) \quad (2.6)$$

Ratios between land volumes must be the same in real case and in the model. But as it can be seen in the above calculations, they are not the same.

$$\frac{V_1}{V_2} \neq \frac{V'_1}{V'_2} \quad \frac{V_1}{V_3} \neq \frac{V'_1}{V'_3} \quad \frac{V_2}{V_3} = \frac{V'_2}{V'_3} \quad (2.7)$$

Land pressures during the combustion cycle have crucial importance in the calculation of the backflow of oil. Therefore the ring length is changed to leave the volumetric ratio of the lands the same as in original 3D geometry.

D_1 is replaced with D'_1 only for V'_1 . Then volumetric ratios remain the same (Fig 2.5).

$$\frac{V_1}{V_2} = \frac{V'_1}{V'_2} \quad \frac{V_1}{V_3} = \frac{V'_1}{V'_3} \quad \frac{V_2}{V_3} = \frac{V'_2}{V'_3} \quad (2.8)$$

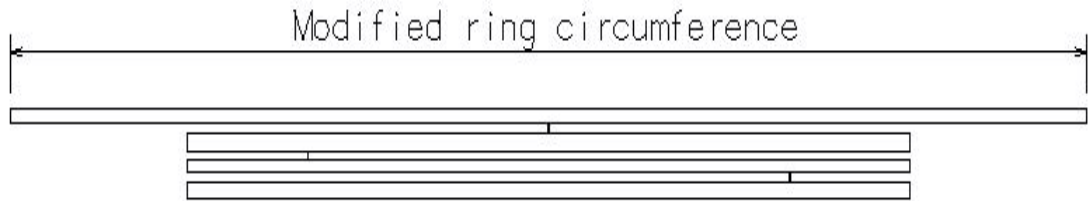


Figure 2.5 Modified 2D geometry (to scale)

2.2 Modeling of Gas Flow

Initially, a 3D model of the gas between piston and cylinder was analyzed. In 3D air flow model, first problem came out because of the land dimensions. Flow through the lands occurs in narrow passage, with thickness to length ratio about 10. To obtain reasonable result, mesh sizes have to be arranged according to the thickness of the passage. If mesh sizes are arranged according to this small thickness, then volumetric mesh quantity gets too high and also solving time gets longer than a month. Afterwards, mesh dimensions were optimized. During optimization, aspect ratio of the meshes gets higher and this causes convergence problems. In addition to that, computers cannot overcome the 3D analysis in a short

time with these meshes also. Because of these computational restrictions and convergence problems, air flow was modeled for a 2D geometry.

After modeling 2D gas geometry in Gambit [19], 2D mesh of the gas according to the predicted flow route was modeled (Fig. 2.6). Since velocity of the gas through the lands and the ring end gaps is high, viscous effects of the gas can be neglected, but compressibility effects have to be included. Explicit solver is offered for high speed unsteady flows by Fluent [18] user manual files. Therefore gas flow is analyzed using a 2D, double precision, unsteady, explicit, inviscid and compressible solver. Inlet of the geometry is the combustion chamber side. Inlet boundary condition is given as “Pressure Inlet” and this inlet pressure is defined in an UDF (User Defined Function). UDF includes combustion chamber pressure in Pascal versus time array. Outlet boundary condition is given as “Pressure Outlet” boundary condition and the magnitude is about atmospheric pressure because the crank case pressure of the engine is close to the atmospheric pressure.

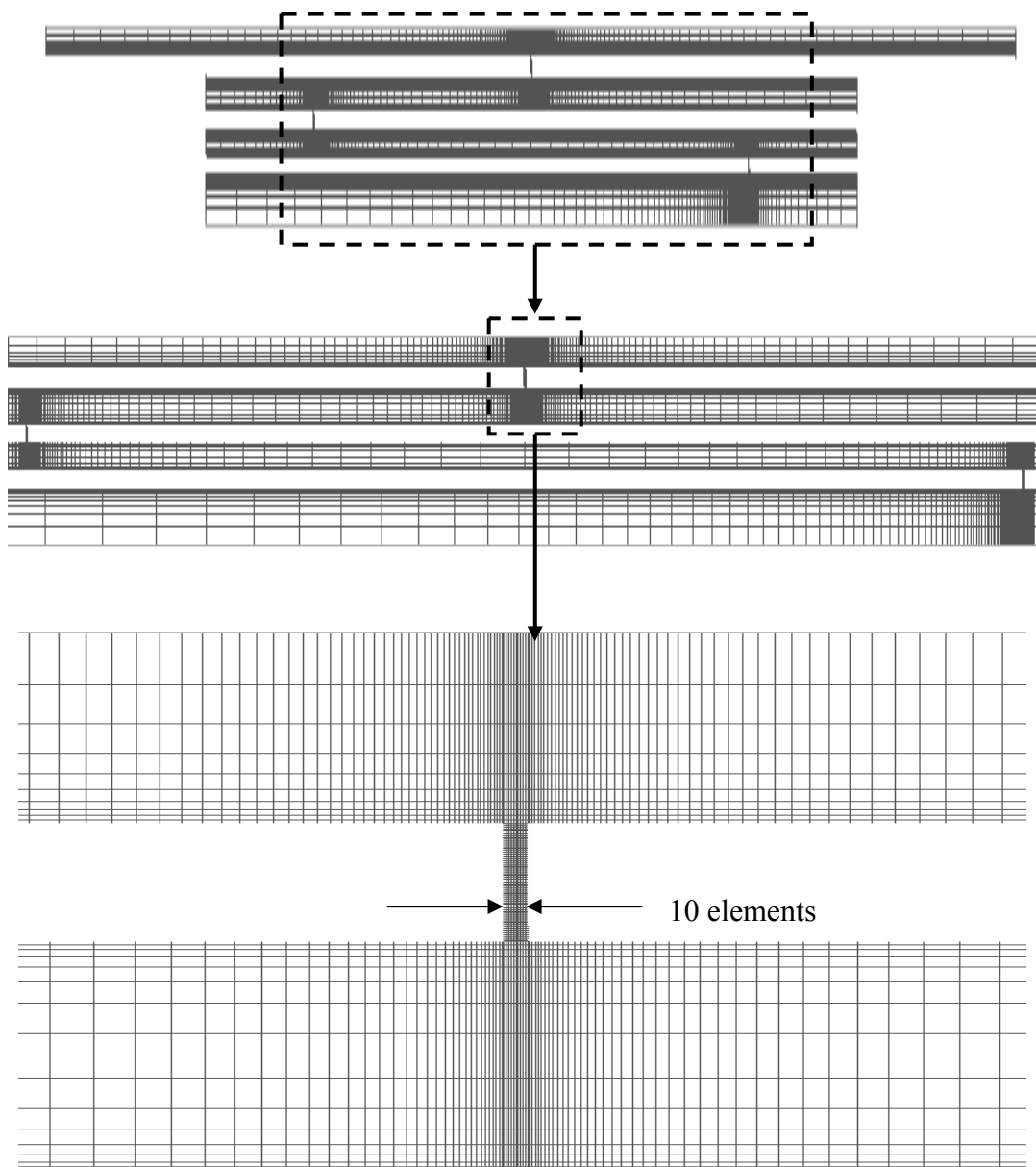


Figure 2.6 2D mesh (11065 cells, 23094 faces and 12075 nodes) (to scale)

All gas flow analysis are run a minimum six cycles to reach cyclic convergence. First check of the cyclic convergence is peak pressure check of the lands. Second check is done by calculating total mass flow rates through the ring end gaps. These mass flow rates converge to a value after five cycles and the sixth cycle data are taken to analyze the oil backflow.

During calculation of the gas mass flow rates, blowby results of the engine are also obtained by integrating gas mass flow rates during last cycle. Blowby results of different engine speeds are given in the results chapter.

Following values are obtained from the Fluent© [18] analysis

Mass flow rates through 1st, 2nd and 3rd ring and gaps,

Average pressures in the 1st, 2nd and 3rd lands,

1st, 2nd and 3rd ring end gap velocities,

1st, 2nd and 3rd ring end gap maximum velocities.

2.3 Oil Gas Interface Velocity

According to the air flow analysis, ring end gaps are determined as a critical region. Therefore oil gas interface velocity is calculated throughout the ring end gap.

In the oil flow model, Reynolds number of oil (Re_{oil}) has an important role in the entrainment rate calculations. Re_{oil} can be described as:

$$Re_{oil} = \frac{\rho_{oil} V_{oil} D_h}{\mu_{oil}} \quad (2.9)$$

In Re_{oil} equation, V_{oil} represents the oil film superficial velocity. In order to calculate the oil film superficial velocity, ring end gap flow is assumed to be a two dimensional pipe flow. Since the gas flows too fast through the ring end gaps, gas flow assumed to be turbulent ($Re_{gas} \sim 4000$). On the other hand, since oil film thickness is too thin (max 5 microns) throughout the ring end gap, oil film flow is assumed to be laminar. Velocity distribution in this two dimensional, two phase pipe flow is shown in Figure 2.7.

Gas Reynolds number, gas and oil velocity profiles are defined as [20].

$$\text{Re}_{gas} = \frac{\rho_{gas} V_{gas} D_h}{\mu_{gas}} \quad (2.10)$$

$$\frac{V_{gas}}{V_{max}} = \left(\frac{y + \delta}{h} \right)^{1/6} \quad (2.11)$$

$$V_{oil} = \frac{1}{2\mu_{oil}} \left(\frac{dP}{dx} \right) y^{*2} + b_1 y^* \quad (2.12)$$

The distance between y and y^* defined as δ . Turbulent velocity profile is displaced from the wall of the ring end gap because of the thin oil film. δ is an unknown in the gas velocity profile. In the oil velocity profile there is also an unknown parameter b_1 , an integration constant. To calculate the unknown parameters, interface velocity can be calculated by using the velocity profiles with the help of boundary conditions which are the continuity of velocity and shear stress at the interface. Detailed information about calculation of interface velocity is given in the Appendix A.

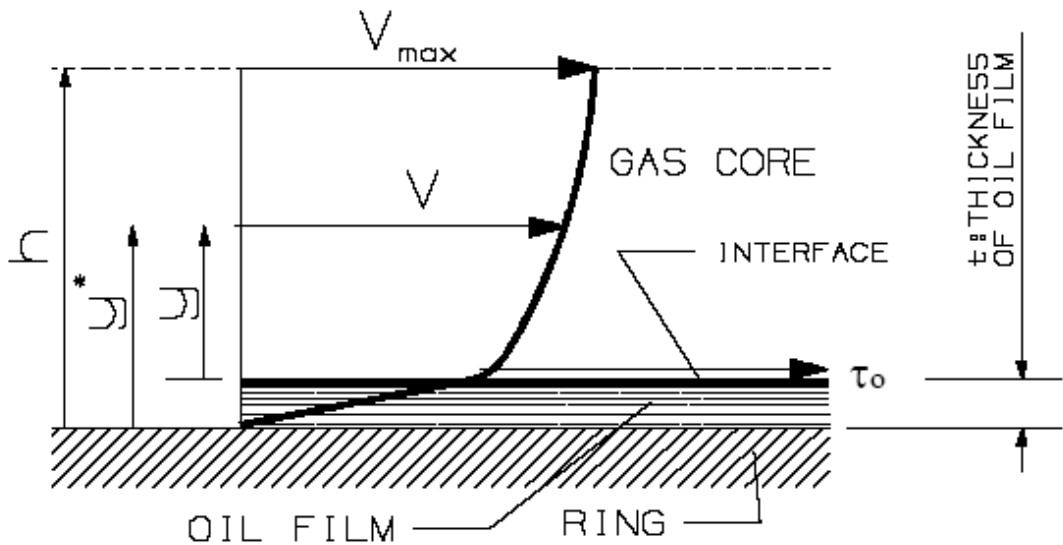


Figure 2.7 Representation of gas flow model [14]

2.4 Oil Flow Model

Table 2.2 Physical properties of fluids

μ_{oil} (Dynamic viscosity of oil)	1.9×10^{-2} N.s/m ²
σ_{oil} (Surface tension of oil)	2.2×10^{-2} N/m
ρ_{oil} (Density of oil)	850 kg/m ³
μ_{gas} (Dynamic viscosity of gas)	2.4×10^{-5} N.s/m ²
ρ_{gas} (Density of gas)	0.84 kg/m ³

Physical properties of oil and air are listed in Table 2.2. Oil flow model is based on the entrainment rate calculation and conservation of mass.

2.4.1 Entrainment rate calculation

Entrainment rate is a crucial problem not only for oil consumption in internal combustion engines but also for the nuclear reactors. Most of the correlations were developed by nuclear engineers for air water two phase flow systems. There is not any correlation in the literature for the mixture of gas oil two phase flows. Therefore air water correlation developed by Kataoka et al. [9] is used for the entrainment rate calculation in this study. Water entrainment into the air by shearing-off roll wave crest constructed the base of this correlation and, shearing-off the roll wave crest starts since interfacial shear force is higher than retaining force of surface tension (Figure 2.8).

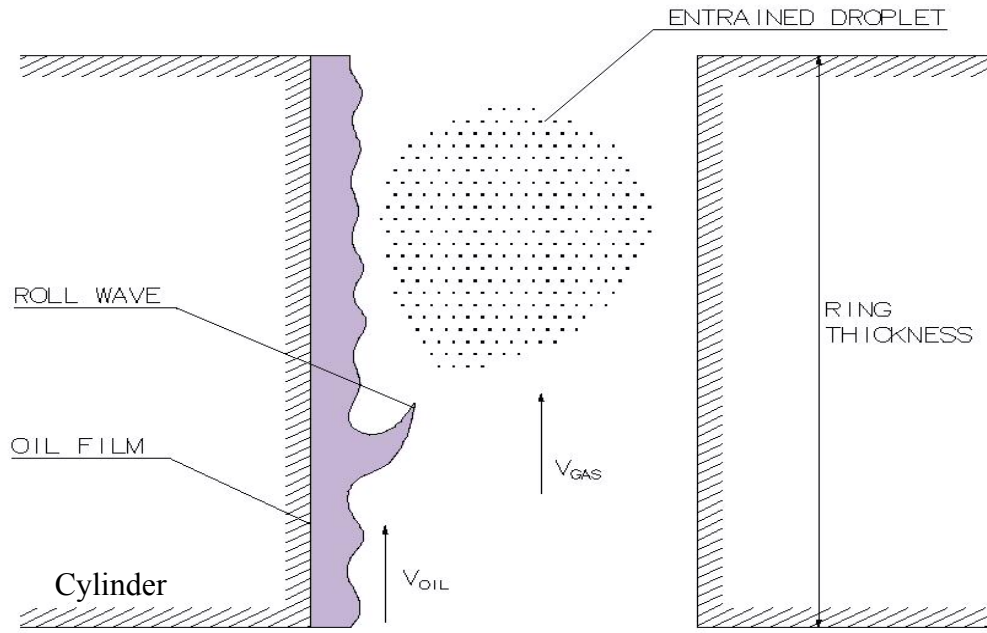


Figure 2.8 Oil entrainment mechanism

Entrainment fraction is defined as

$$E = \frac{\dot{m}_{ent}}{\dot{m}_{oil}} = \frac{J_{ent}}{J_{oil}} \quad (2.13)$$

where \dot{m}_{ent} , \dot{m}_{oil} , J_{ent} and J_{oil} are droplet mass flow rate, total oil mass flow rate, droplet volumetric flux and total oil volumetric flux, respectively. Entrainment fraction can be defined also in terms of oil Reynolds number and modified Weber number as follows

Oil Film Reynolds number:

$$Re_{oil} = \frac{\rho_{oil} V_{oil} D_h}{\mu_{oil}} \quad (2.14)$$

Modified Weber number:

$$We = \frac{\rho_{gas} V_{gas} D_h}{\sigma_{oil}} \left(\frac{\rho_{oil} - \rho_{gas}}{\rho_{gas}} \right)^{1/3} \quad (2.15)$$

Entrainment fraction:

$$E = \tanh\left(7.25 \times 10^{-7} We^{1.25} Re_{oil}^{0.25}\right) \quad (2.16)$$

Where D_h is hydraulic diameter and defined as

$$D_h = \frac{4R_g R_r}{2(R_g + R_r)} \quad (2.17)$$

$$R_r = (D_1 - D_3)/2 \quad (2.18)$$

With the help of hydraulic diameter, oil film Reynolds number, modified Weber number and entrainment fraction, entrainment rate can be calculated in $\text{kg/m}^2 \cdot \text{s}$.

Entrainment rate:

$$\dot{\epsilon} = 0.935 \times 10^{-5} \zeta \exp\left(-1.87 \times 10^{-5} \zeta^2\right) \rho_{oil} V_{oil} Re_{oil}^{0.5} We^{-0.25} E \quad (2.19)$$

$$+ 0.022 \rho_{oil} V_{oil} Re_{oil}^{-0.26} \left(\frac{\mu_{gas}}{\mu_{oil}}\right)^{0.26} E^{0.74} \times \left(1 - \exp\left(-1.87 \times 10^{-5} \zeta^2\right)\right)^{0.74}$$

where ζ is axial dimensionless distance from the beginning of the ring end gap:

$$\zeta = \frac{(z/D_h) Re_{oil}^{0.5}}{We^{0.25}} \quad (2.20)$$

Total entrained oil mass flow through the ring is calculated by integrating over the entire surface from the beginning to the end of the ring end gap passage (Figure 2.9):

$$\dot{m}_{oil} = R_g \int_0^{R_t} \dot{\epsilon} dz \quad (2.21)$$

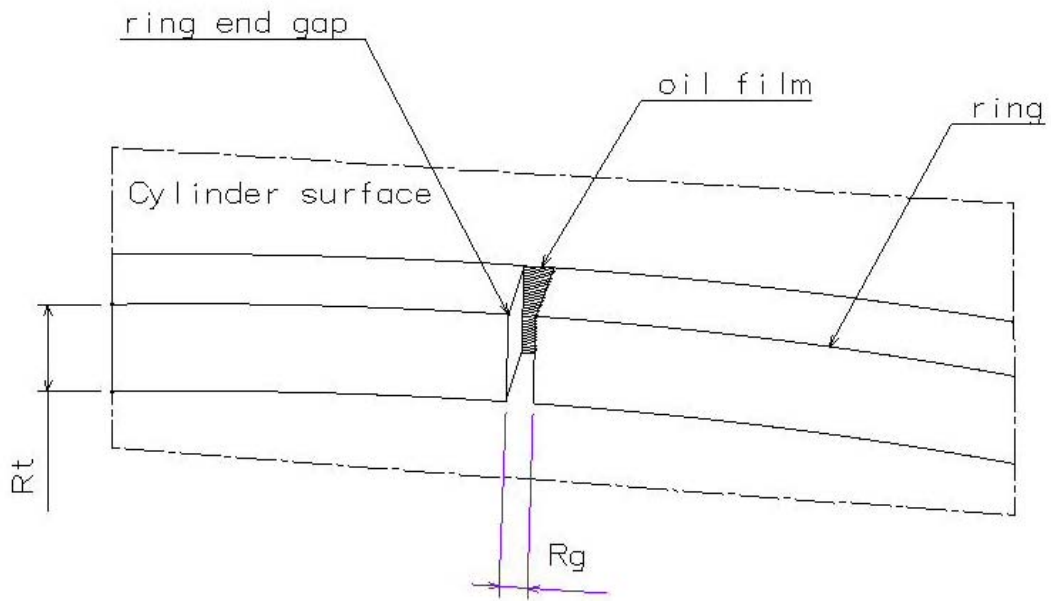


Figure 2.9 Ring end gap and oil film

2.4.2 Conservation of mass for oil

Piston cylinder assembly consists of two main lands called 2nd and 3rd land. Oil mass of the whole system is conserved during the operation of the engine, which means that mass of the oil has cyclic independency of time and is represented as

$$\frac{dm_{system}}{dt_{cycle}} = 0 \quad (2.22)$$

Conservation of mass also applies to subsystems, 2nd and 3rd land.

$$\frac{dm_{oil2}}{dt_{cycle}} = 0 \quad (2.23)$$

$$\frac{dm_{oil3}}{dt_{cycle}} = 0 \quad (2.24)$$

As previously explained, oil is entrained from the ring end gap oil film. According to pressures of the lands some entrained oil is accumulated in the lands and accumulated oil flows between lands or from lands to the combustion chamber or to

the crankcase. To explain conservation of oil, oil transfer between the lands, combustion chamber and lands are explained below.

Accumulated oil change in the 2nd land during the cycle:

$$\frac{dm_{oil2}}{dt} = \dot{m}_{ent1} + \dot{m}_{ent2} + \dot{m}_{21} + \dot{m}_{23} \quad (2.25)$$

Accumulated oil change in the 3rd land during the cycle:

$$\frac{dm_{oil3}}{dt} = \dot{m}_{ent2} + \dot{m}_{ent3} + \dot{m}_{32} + \dot{m}_{34} \quad (2.26)$$

Total oil in the 2nd land on time t_1 of the cycle

$$m_{oil2,t_1} = \sum_{t=t_0}^{t_1} (\dot{m}_{ent1,t} + \dot{m}_{ent2,t} + \dot{m}_{21,t} + \dot{m}_{23,t}) \quad (2.27)$$

Total oil in the 3rd land on time t_1 of the cycle

$$m_{oil3,t_1} = \sum_{t=t_0}^{t_1} (\dot{m}_{ent2,t} + \dot{m}_{ent3,t} + \dot{m}_{32,t} + \dot{m}_{34,t}) \quad (2.28)$$

Accumulated oil transfer from 2nd land to the combustion chamber on time t_1 of the cycle

$$m_{21,t_1} = \frac{m_{oil2,t_1} V_1 A_1}{V_2} \quad (2.29)$$

Accumulated oil transfer from 2nd land to the 3rd land on time t_1 of the cycle

$$m_{23,t_1} = \frac{m_{oil2,t_1} V_2 A_2}{V_2} \quad (2.30)$$

Accumulated oil transfer from 3rd land to the 2nd land on time t_1 of the cycle

$$m_{32,t_1} = \frac{m_{oil3,t_1} V_2 A_2}{V_3} \quad (2.31)$$

Accumulated oil transfer from 3rd land to the crankcase on time t_1 of the cycle

$$m_{34,t_1} = \frac{m_{oil3,t_1} V_3 A_3}{V_3} \quad (2.32)$$

Oil mass transfer and oil accumulation in the lands are calculated for the whole cycle. After each cycle, calculations are repeated with the previous cycle data till the oil mass converges.

CHAPTER 3

RESULTS AND DISCUSSION

In this chapter, results of the gas and oil flow analysis are presented. Land pressure variations, maximum land pressure values and blowby percentages are given as gas flow analysis result. In the second part of this chapter, oil blowback parametric study results are examined. These results are compared with the previous experimental and numerical studies.

3.1 Gas Flow Analysis Results

The result of the 2100 rpm full load case is compared with the previous research [14] to validate the analysis method (Figure 3.1). Figure 3.1 shows that, 2nd and 3rd land pressure variations are very close to each other. 2nd land pressure variation and maximum pressure values are nearly the same. 3rd land maximum pressure values and crank angle of the maximum pressure is similar but not as close as 2nd land. The result of the comparison is that the tendencies of the pressure variations for 2nd and 3rd lands are acceptable to continue the following analysis.

According to the combustion chamber pressure variation, 2nd and 3rd land pressure variations are examined at different engine operation conditions, from 900 rpm to 2100 rpm with 200 rpm step. 2100 rpm, 1500 rpm and 900 rpm results are given in Figure 3.2 (a), (b) and (c), respectively. 2100 rpm engine operation condition is taken as base in this thesis.

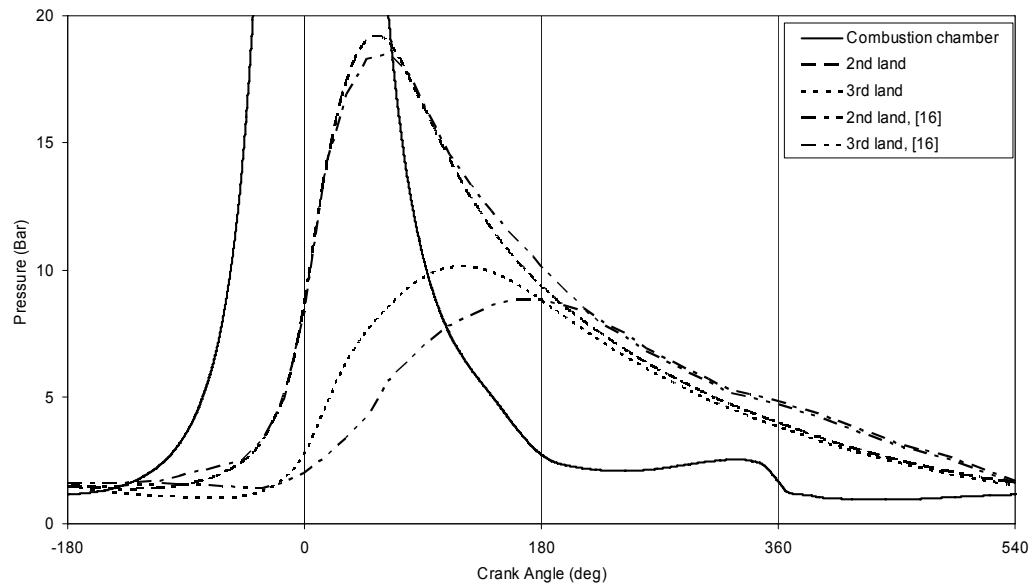
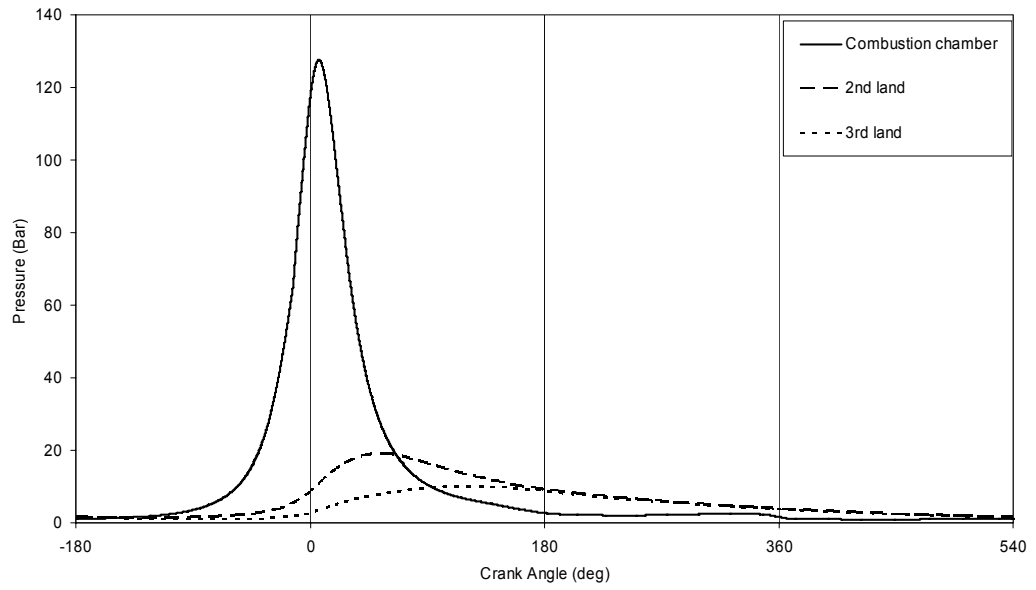


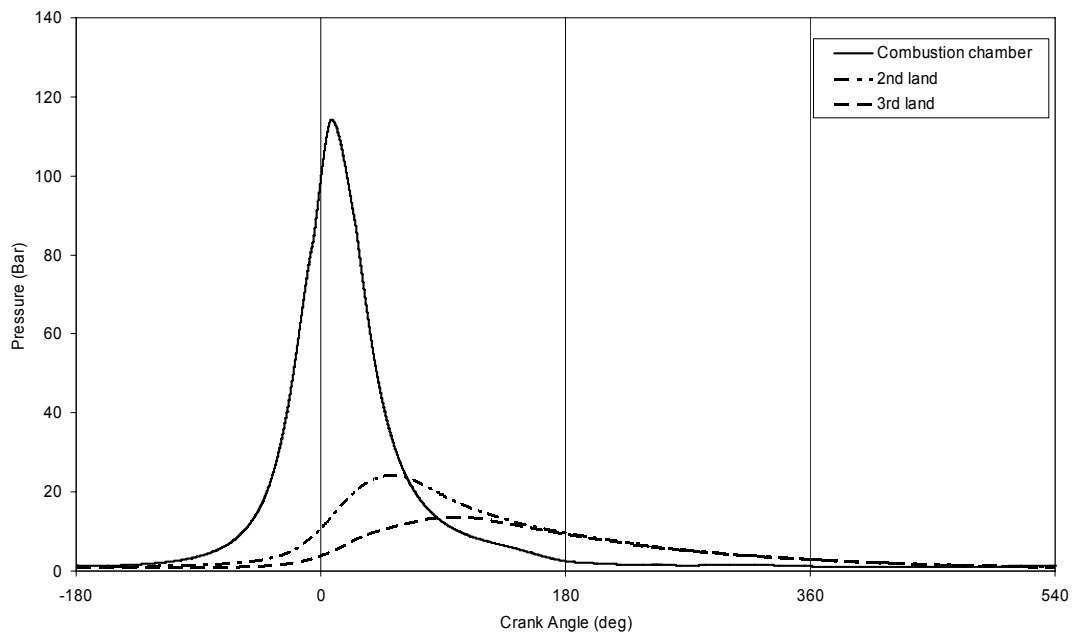
Figure 3.1 Land volume pressures at 2100 rpm, full load (comparison with [14])

In current analysis results, in Figure 3.2 (a), (b) and (c), combustion chamber pressure increases rapidly because of the compression motion of the piston and combustion of the diesel fuel. But 2nd and 3rd land pressure can not increase as quickly as combustion chamber. Because of the rings orientation and small ring end gap thicknesses, 2nd land pressure increases more quickly than 3rd land pressure. After 6° of the crank, combustion chamber pressure decreases rapidly because of the expansion motion of the piston. But 2nd and 3rd land pressures cannot decrease as quickly as combustion chamber. Due to the higher pressure in the 2nd land with respect to the combustion chamber, gas flows through the 1st ring end gap to the combustion chamber.

2nd land pressure exceeds the combustion chamber pressure at about 60° of the crank. The start of pressurization during the compression, and depressurization in late exhaust strokes of the 2nd land is nearly the same in all engine speeds, although combustion chamber maximum pressures are different. According to the engine speeds; at 2100 rpm, 1500 rpm and 900 rpm, a cycle of the engine (720°) takes about 0.057s, 0.080s and 0.133s, respectively.

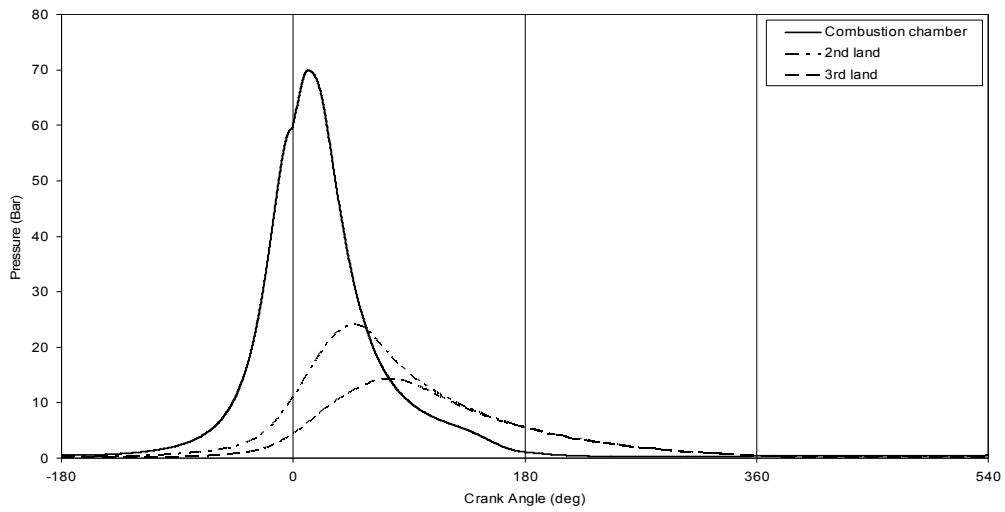


(a) 2100 rpm full load



(b) 1500 rpm full load

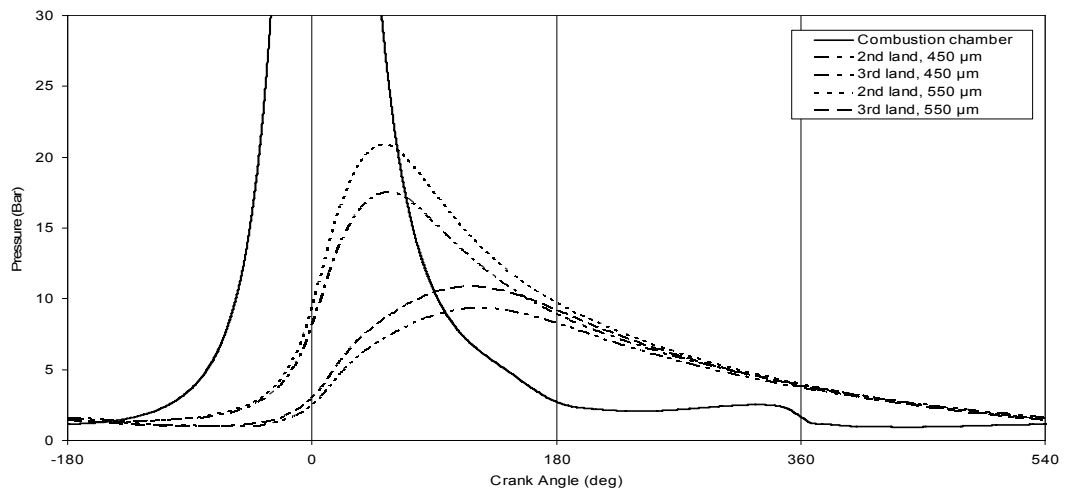
Figure 3.2 Land volume pressures at 500 μm top ring end gap



(c) 900 rpm full load

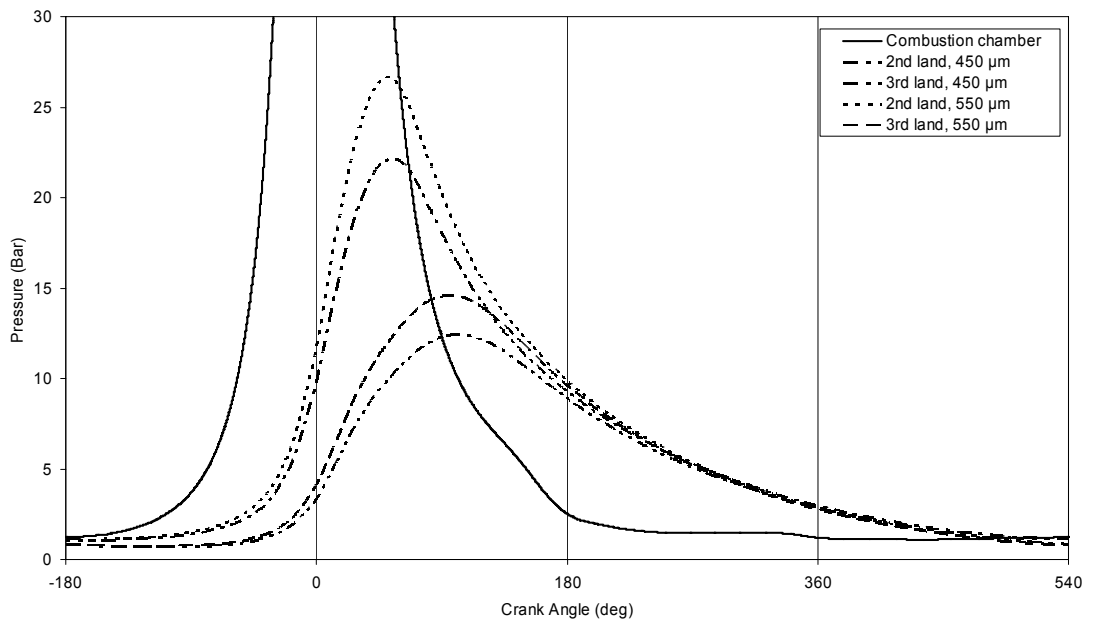
Figure 3.2 Land volume pressures at 500 μm top ring end gap (Continued)

In Figure 3.3 (a), (b) and (c), 2nd and 3rd land pressure variations can be seen at 2100 rpm, 1500 rpm and 900 rpm engine operation conditions and for 450 μm and 550 μm ring end gaps. Change of the ring end gap does not affect the pressurization and depressurization time of the 2nd and 3rd land much. It only affects gas mass flow rate, because of pressure variation of the lands.

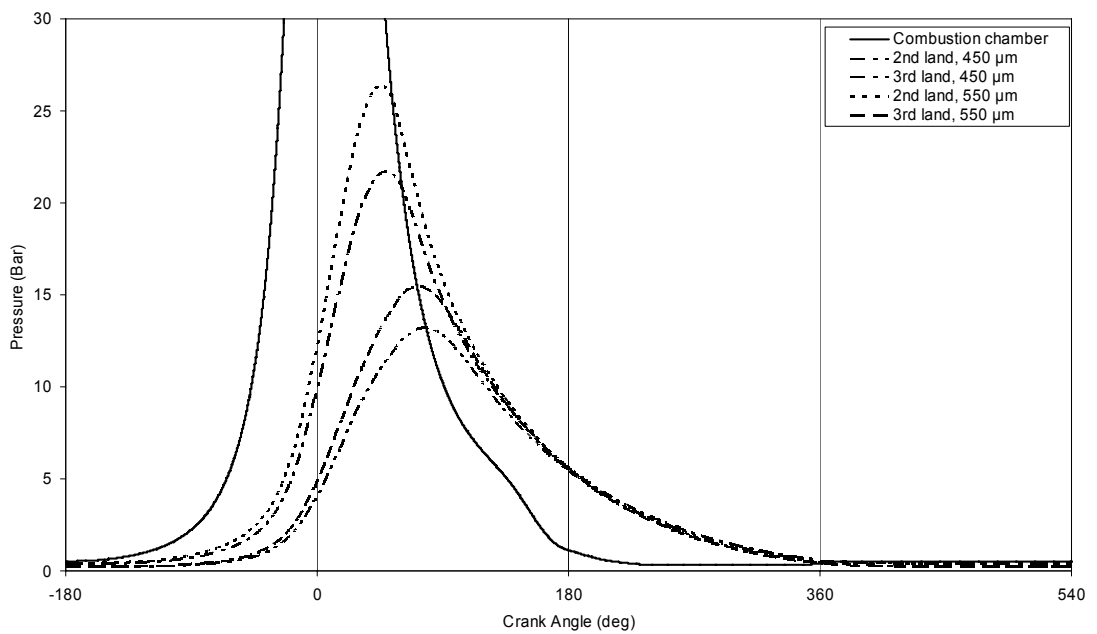


(a) 2100 rpm full load

Figure 3.3 Land volume pressures at different top ring end gaps



(b) 1500 rpm full load



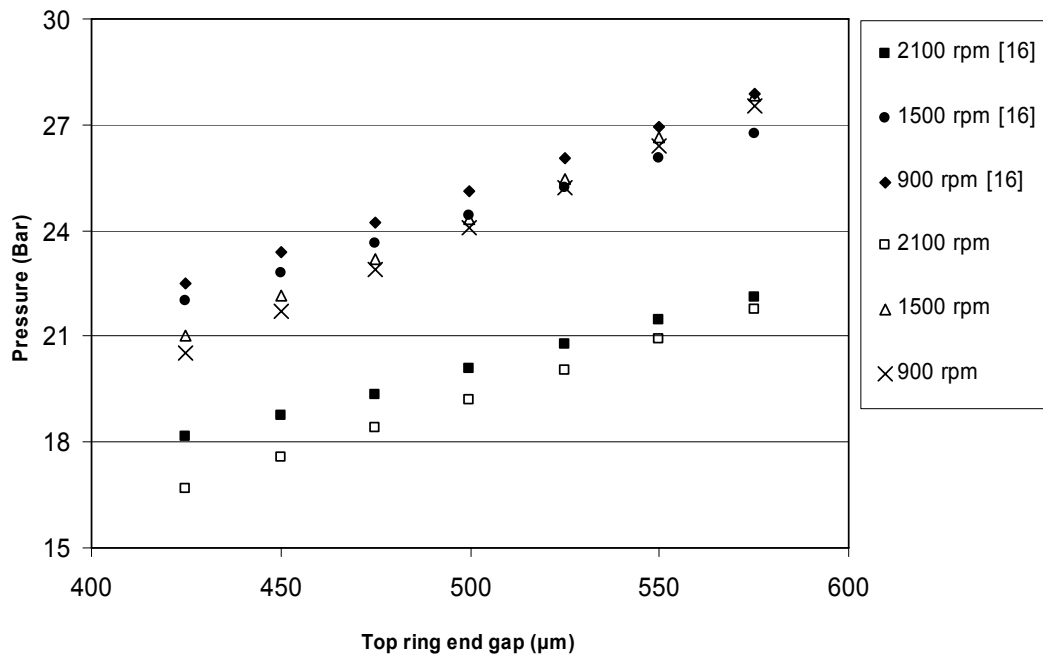
(c) 900 rpm full load

Figure 3.3 Land volume pressures at different top ring end gaps (Continued)

As it is seen in Figure 3.4 (a) and Figure 3.5 (a), in comparison of [14] and the current study of the 2nd and 3rd land maximum pressures at 2100 rpm, 1500 rpm and

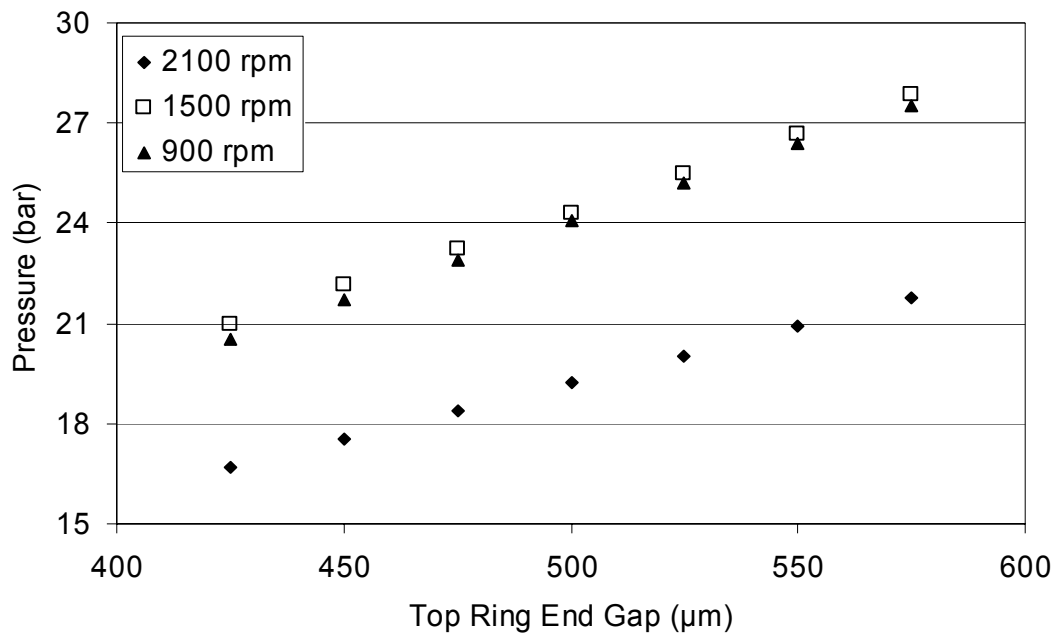
900 rpm full load engine operation condition are presented for different top ring end gaps, from 425 μm to 575 μm with 25 μm increment. The comparisons show that previous research and the current study give similar results.

In Figure 3.4 (b) it is shown that how the maximum pressure of the 2nd land is affected by the change of the top ring end gap. As a result, increase of the top ring end gap is proportional to the 2nd land maximum pressure.



(a) 2nd land peak pressure (comparison with Karkaç [14])

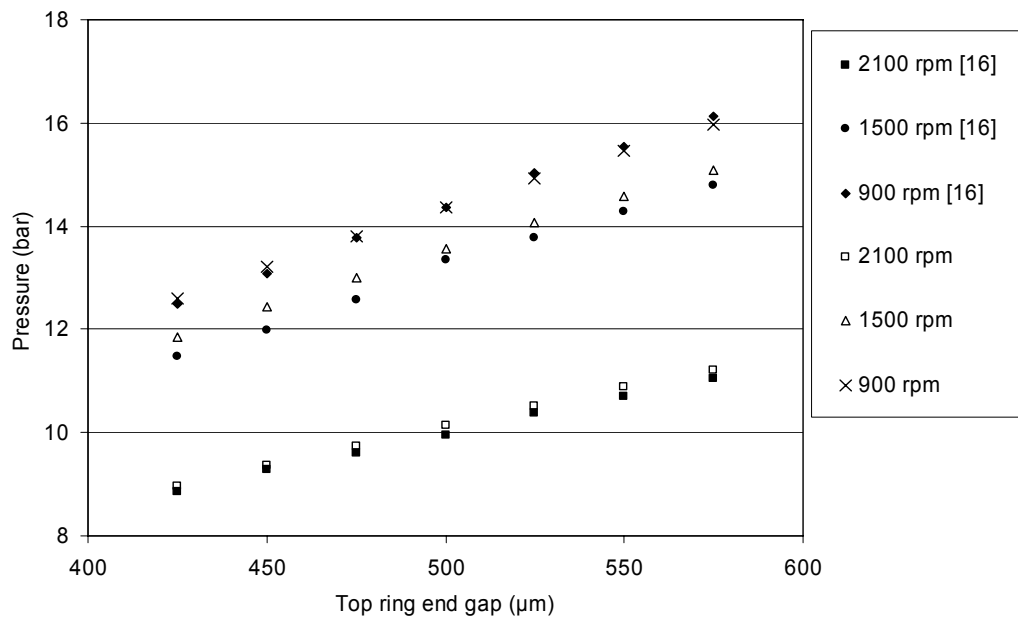
Figure 3.4 2nd land peak pressures at different top ring end gaps



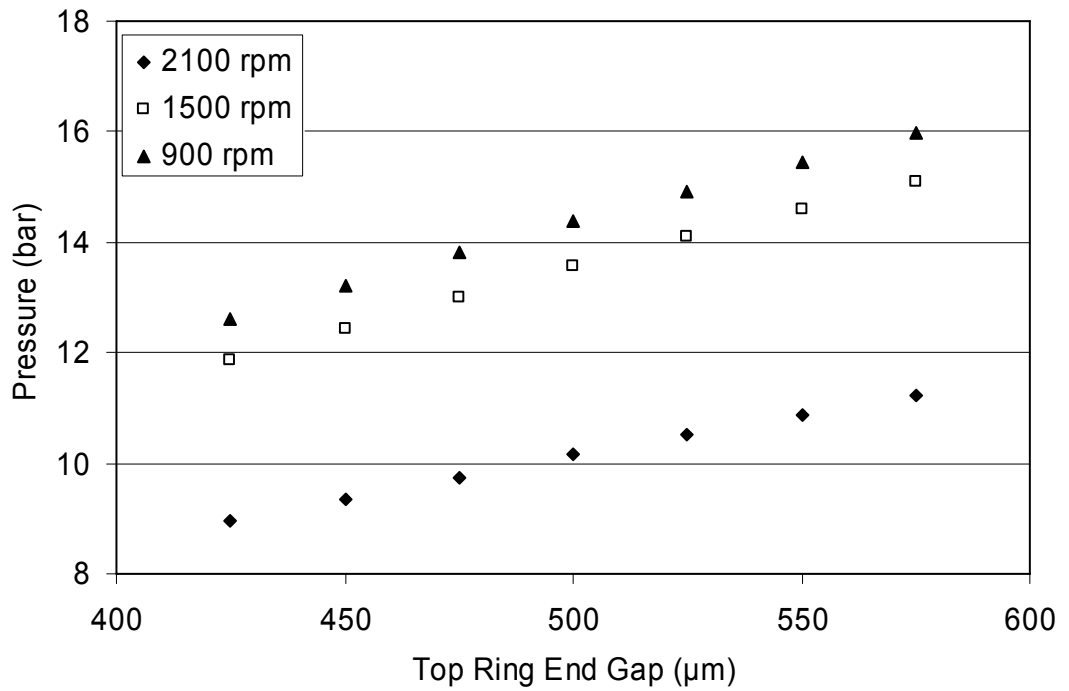
(b) 2nd land peak pressures (current study)

Figure 3.4 2nd land peak pressures at different top ring end gaps (Continued)

3rd land maximum pressure at 900 rpm is higher than 1500 rpm and 2100 rpm engine operation conditions (Fig. 3.5 (b)) since the combustion chamber pressure of 900 rpm is lower than 1500 rpm and 2100 rpm engine operation condition. Pressurization time of 3rd land is higher at 900 rpm engine operation condition than 1500 rpm and 2100 rpm engine operation conditions.



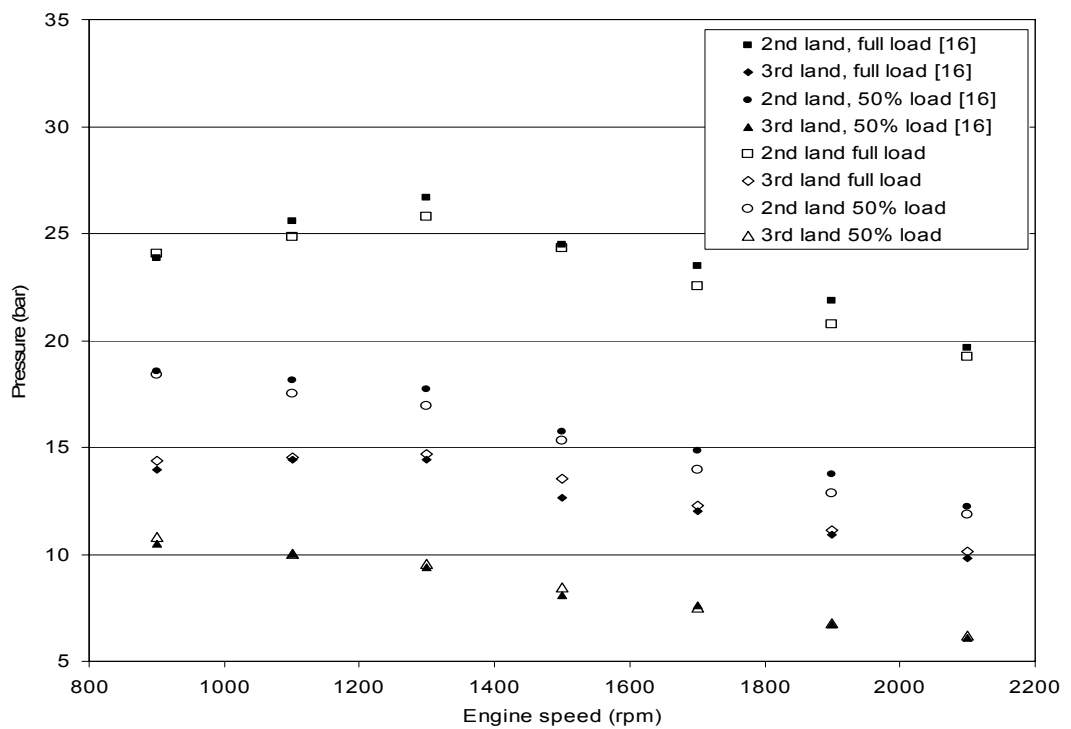
(a) 3rd land volume peak pressure (comparison with Karkaç [14])



(b) 3rd land peak pressures (current study)

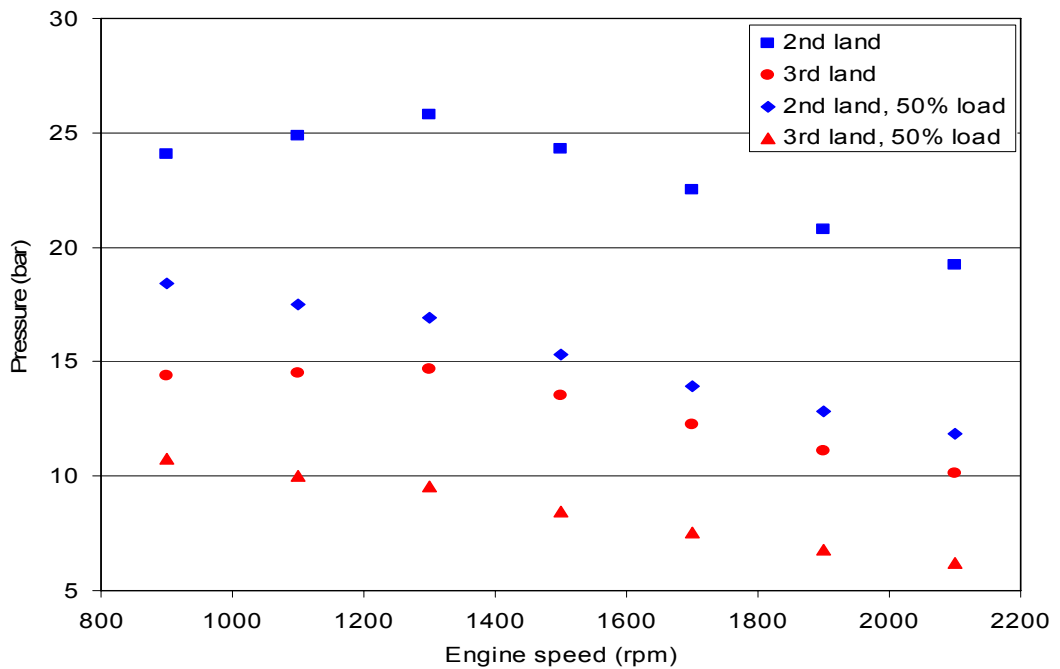
Figure 3.5 3rd land peak pressures at different top ring end gaps

The comparison of Karkaç [14] and the current study results for the maximum land pressures at different engine operation conditions and different engine loads are given in the Figure 3.6 (a). In Figure 3.6 (b) current study results are given. Figure 3.6 (a) shows that Karkaç [14] and current study results are very close to each other. From Figure 3.6 (b) it is found that at 1300 rpm full load engine operation condition 2nd and 3rd land maximum pressures are higher than the other operation conditions and loads. But for the 50% load condition, 2nd and 3rd land pressures are higher than the other engine operation conditions at 900 rpm.



(a) Land volume peak pressure (comparison with Karkaç [14])

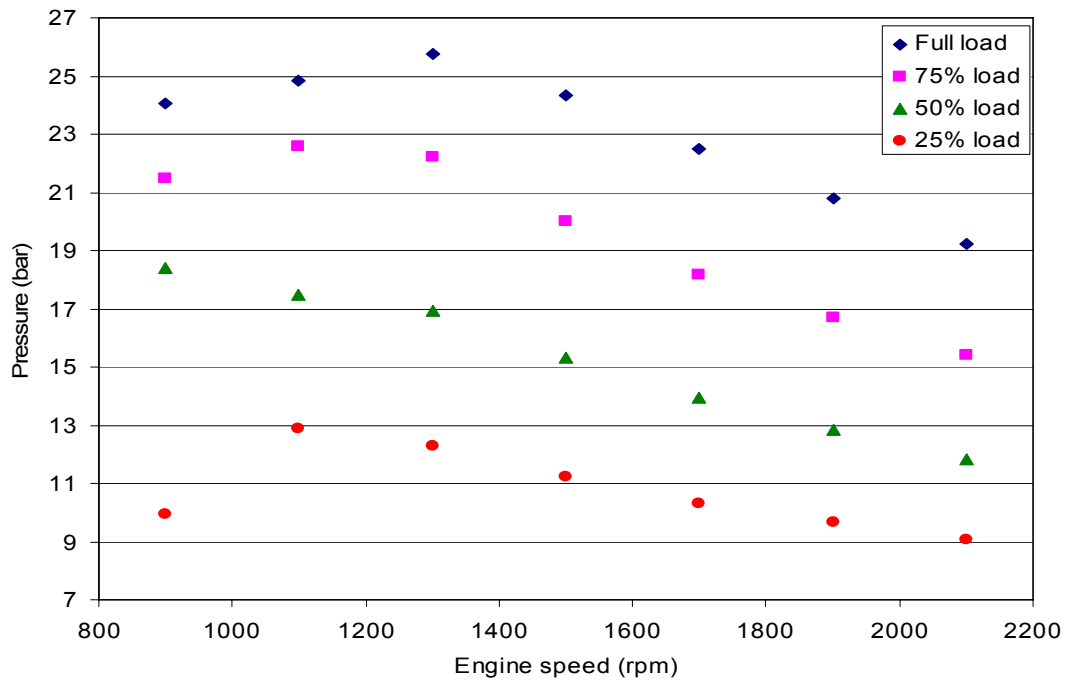
Figure 3.6 Land volume peak pressures at full and 50% load



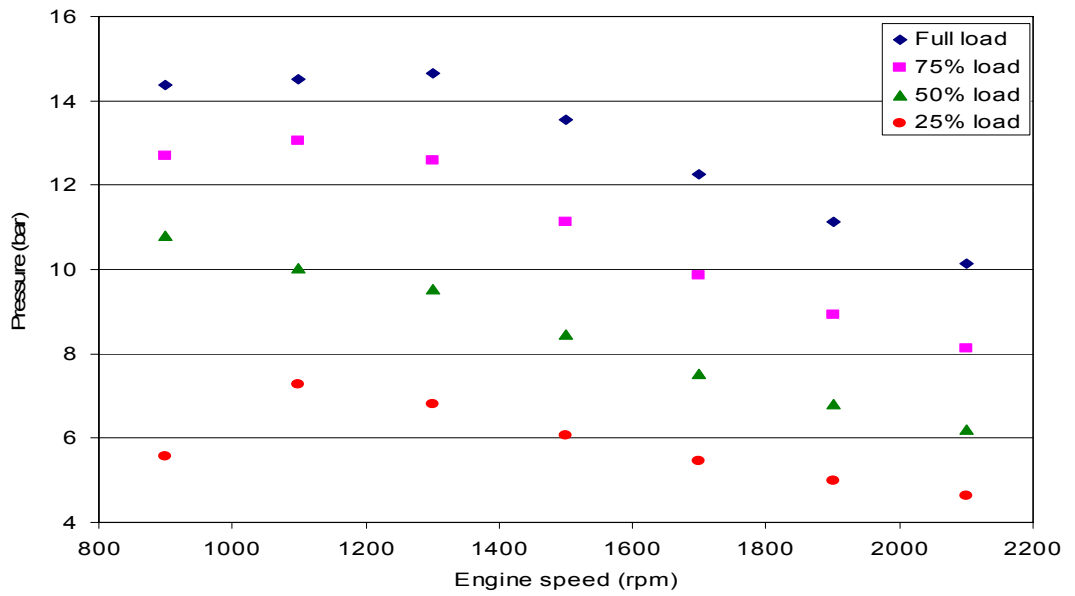
(b) Calculated land volume peak pressures (current study)

Figure 3.67 Land volume peak pressures at full and 50% load (Continued)

2nd and 3rd land maximum pressures at different engine loads and at different engine operation conditions are given in the Figure 3.7 (a) and (b), respectively. At full, 75% and 50% engine loads can be predicted results according to the references [14]. But actually, 25% load 900 rpm engine operation condition result cannot be expected. Pressurization time of the lands is not very different between full, 75%, 50% and 25% engine loads. Maximum combustion chamber pressures of full, 75%, 50% and 25% loads 900 rpm engine operation conditions are 71, 64, 54 and 42 bars, respectively. In order to explain the large land pressure differences observed at 900 rpm engine operation condition between the loads, Mach number of the first ring end gap flow is examined. At the pressurization part of the 2nd land, Mach number is higher than 1 during 0.0215s, 0.0190s, 0.0215s and 0.0166s at full, 75%, 50% and 25% engine loads, respectively. At the backflow, Mach number is higher than 1 during 0.0230s, 0.203s, 0.0180s and 0.0262s at full, 75%, 50% and 25% engine loads, respectively. From these results, lower 2nd and 3rd land pressure for 25% load 900 rpm engine operation condition can be meaningful.



(a) 2nd land



(b) 3rd land

Figure 3.7 Land volume peak pressures at different engine loads

Blowby results at different engine operation conditions and at different loads can be seen on Figure 3.8. Maximum blowby occurs at full load 900 rpm engine operation condition. In all loads, except 25%, blowby is maximum at 900 rpm engine speed. But at 25% load maximum blowby occurs at 1100 rpm engine speed. Exception of 25% load and 900 rpm engine speed condition is explained before.

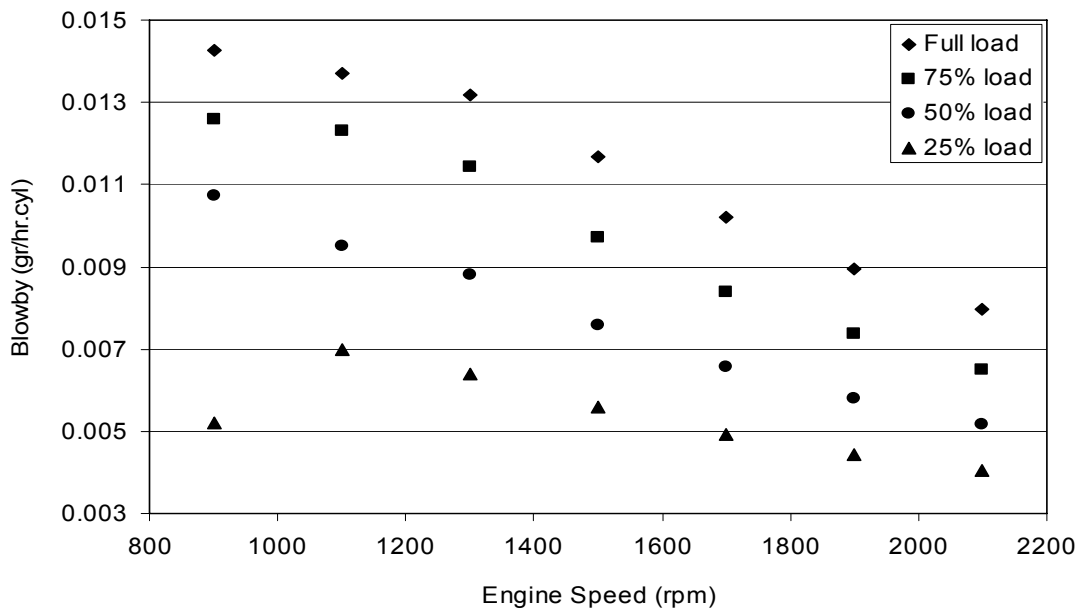
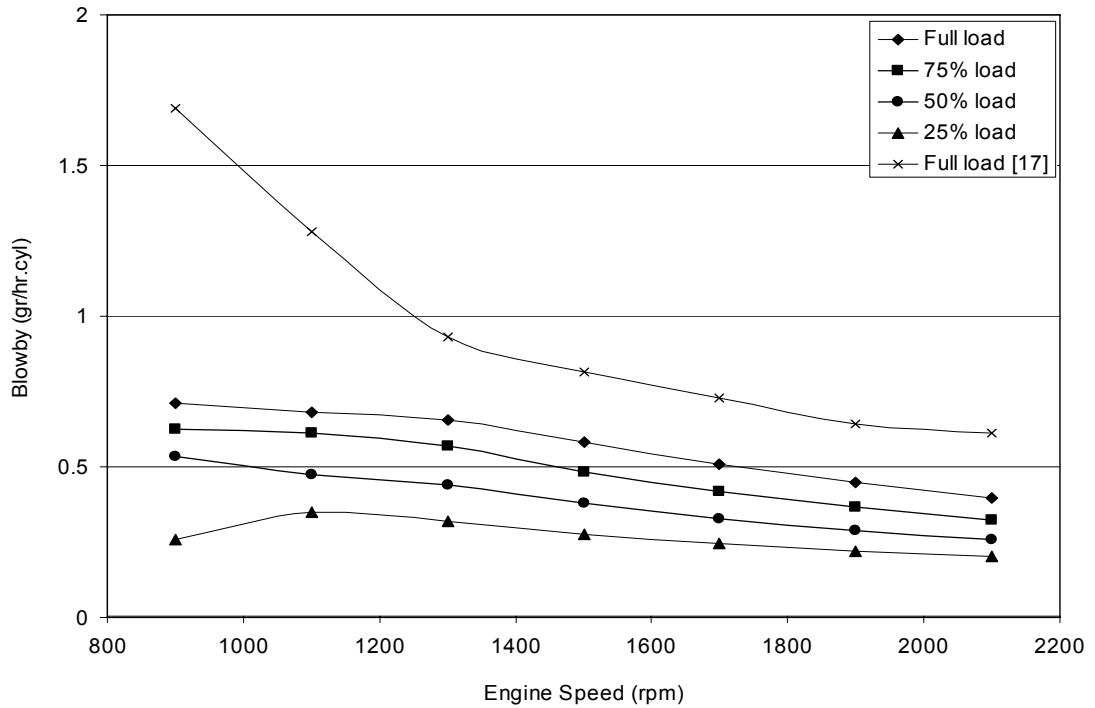


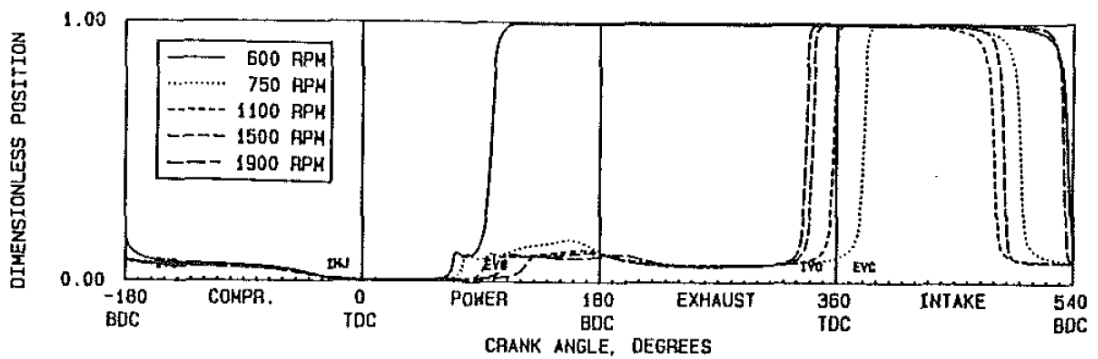
Figure 3.8 Blowby (at different engine loads)

In the Figure 3.9 (a) blowby results are compared with Keribar et al. [15] From 2100 rpm to 1300 rpm tendencies of the blowby are similar. After 1300 rpm, till 900 rpm, difference between the blowby results are too much. The basic difference between the current study and Dursunkaya et al. [15] is that in [15] ring dynamics has been taken into consideration. This can be seen by evaluating Figure 3.9 (a) and (b) together. Except the 600 rpm engine speed, top ring starts moving upward in the power stroke and after going 10-20% of groove, movement of top ring has been stopped with oscillation. At the end of exhaust or early intake stroke, top ring continues the upward motion till the top of the groove. Angle from the start to the end of the motion is large at the slower engine speeds. If top ring is between the top and the bottom of the groove, ring can be tilted or twisted and a big gap is opened

between the piston and the top ring. This gap is much larger than the ring end gap. Therefore, due to the increased gas flow area the model with ring dynamics predicts higher blowby values.



(a) Blowby (comparison with Dursunkaya et al. [15])



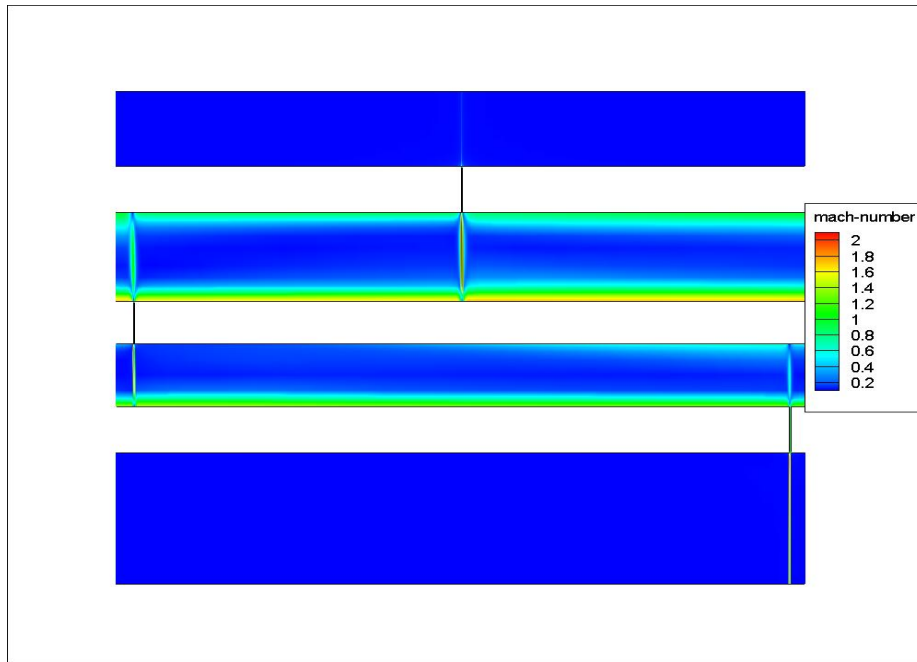
(b) Effect of speed on top ring axial motion, at full load [15]

Figure 3.9 Effect of speed on blowby and top ring axial motion, at full load [15]

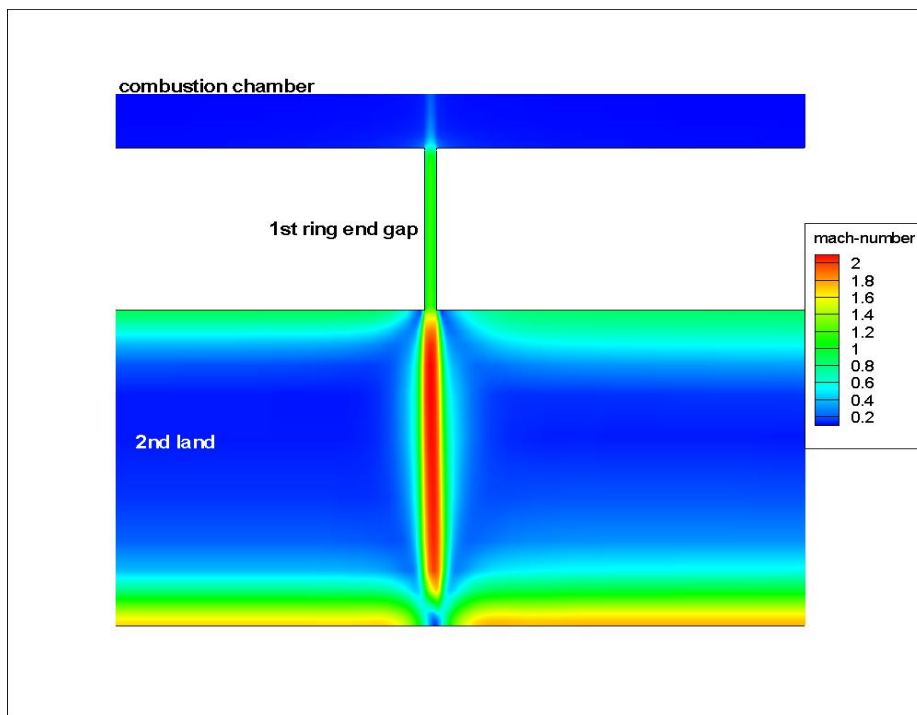
In [14], three volumes represent combustion chamber, 2nd and 3rd lands. These lands are connected with ring end gaps. Flow through the ring end gaps are

simulated by one-dimensional orifice flow. Besides, choked flow assumption is used for the ring end gap flow. By using conservation of mass, land pressures are predicted. But in the current research, two-dimensional analysis model is used to obtain land pressures and ring end gap flow characteristics. In this study, flow Mach number can exceed one, which means flow can be supersonic. In the following figures, detailed view of flow path and flow Mach number can be seen.

In Figure 3.10 (a), (b), (c) and (d) full load, 2100 rpm engine operation condition at maximum combustion chamber pressure Mach contours are given. In Figure 3.10 (b) and (c) Mach contours at first ring end gap can be seen. Because of high pressure ratio between combustion chamber and 2nd land pressures (~ 10) supersonic flow is observed in the first ring end gap. After the first ring end gap, flow speeds up and hit the second ring. Flow divides into two and flows near the upper face of the second ring in the 2nd land. At the second land side of the second ring, gas flows come across and one part of them flows through the second ring end gap to the 3rd land and the other parts form two different circulation patterns in the 2nd land. Since rings are oriented by 120° angle according to the ring end gaps, one circulation covers 120° angle, and the other one covers 240° angle. In Figure 3.10 (c) first ring end gap side of the circulations can be seen. In Figure 3.10 (d) first ring end gap supersonic flow can be seen. Flow is supersonic after entering the ring end gap. Mach number of the flow increases after the first ring end gap like the expansion side of a nozzle. Most of the flow occurs at the sides of the rings in supersonic conditions.

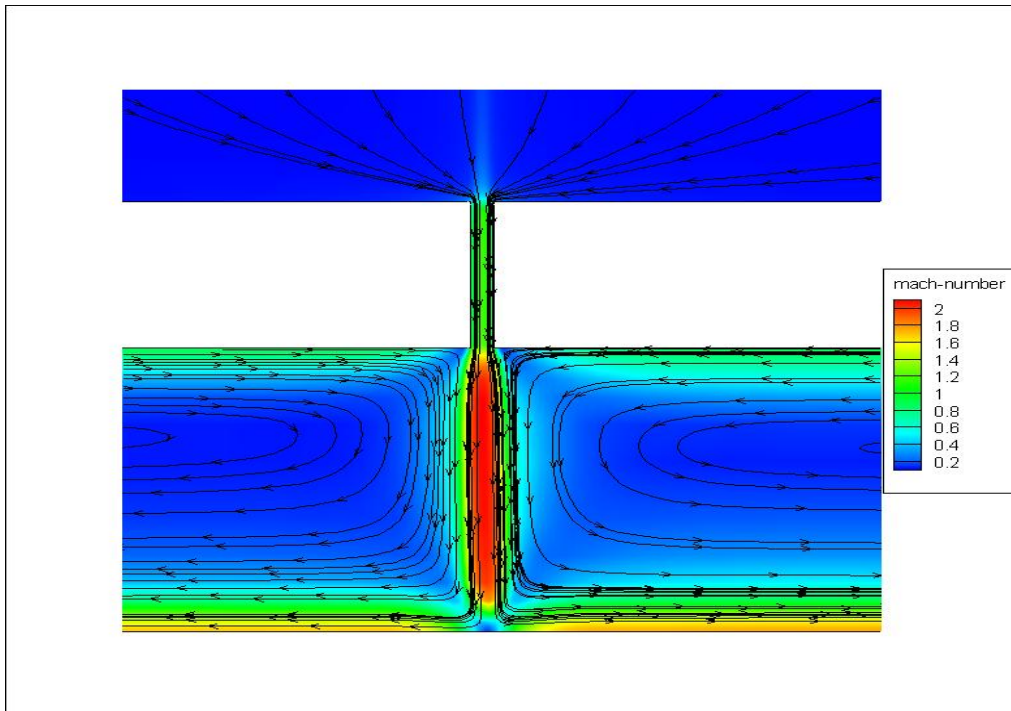


(a) Mach contours (not to scale)

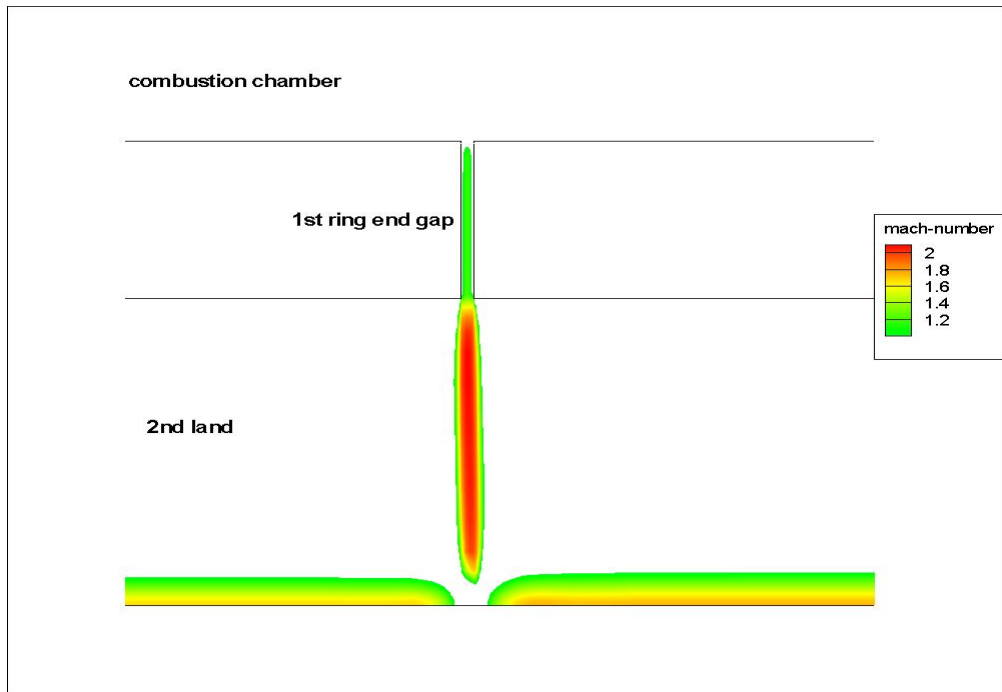


(b) Mach contours (1st ring end gap)

Figure 3.10 Mach contours at maximum combustion chamber pressure (2100 rpm, full load)



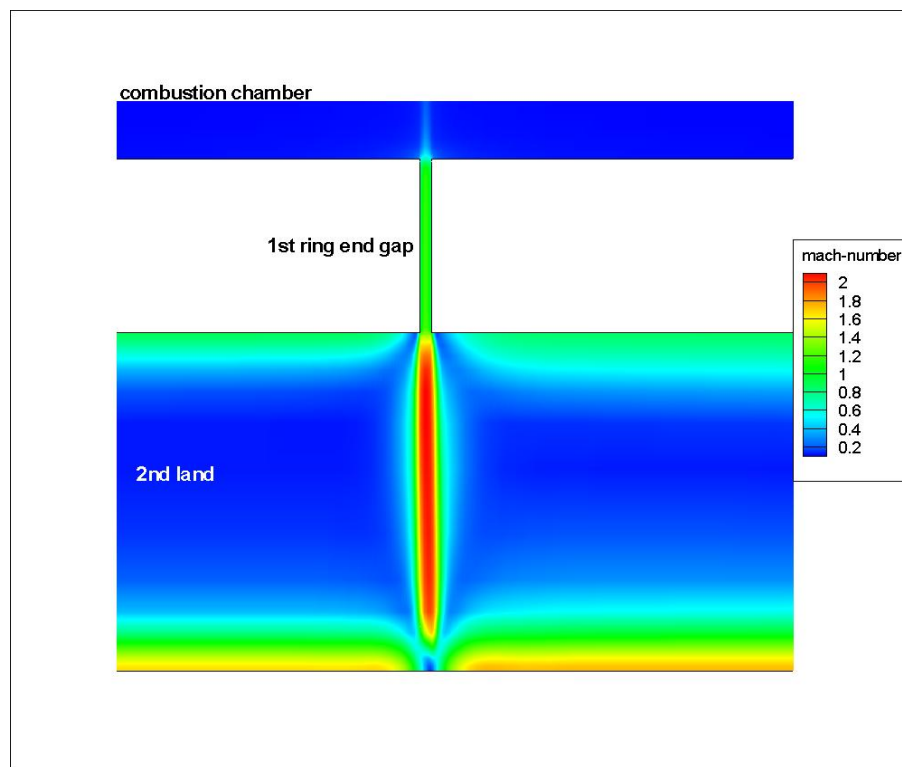
(c) Streamlines (1st ring end gap)



(d) Mach > 1 (1st ring end gap)

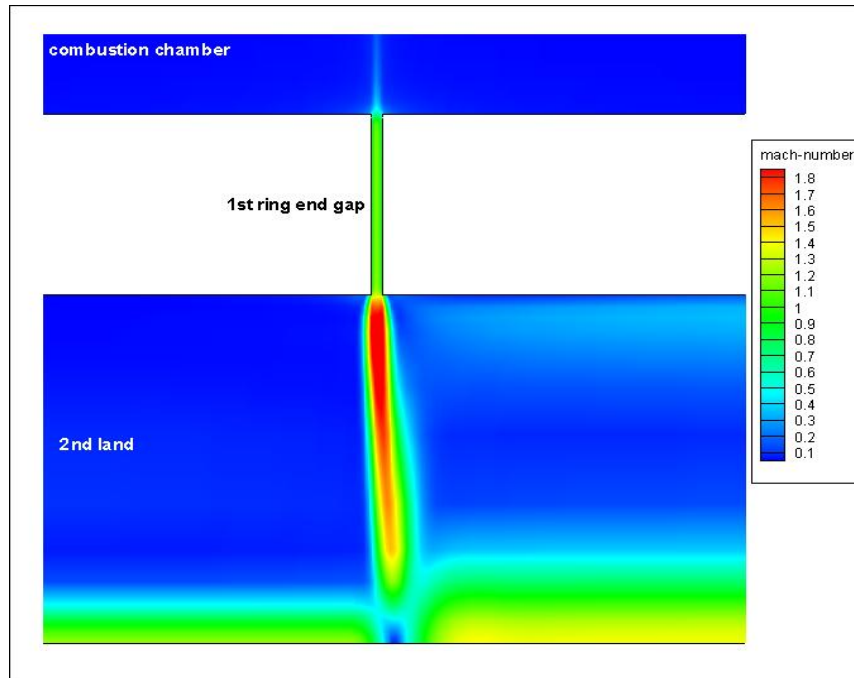
Figure 3.10 Mach contours at maximum combustion chamber pressure
(2100 rpm, full load) (Continued)

In Figures 3.11 (a) and (b), Mach contours at maximum combustion chamber pressure can be seen for inviscid and laminar cases. In this study all analysis are inviscid. If Figures 3.11 (a) and (b) evaluated together, there is no big difference. In both figures, flow can be supersonic after the ring end gap and most of the air flows 2nd land side of the second ring. Besides, 2nd and 3rd land maximum pressure values are neraly the same.



(a) Inviscid

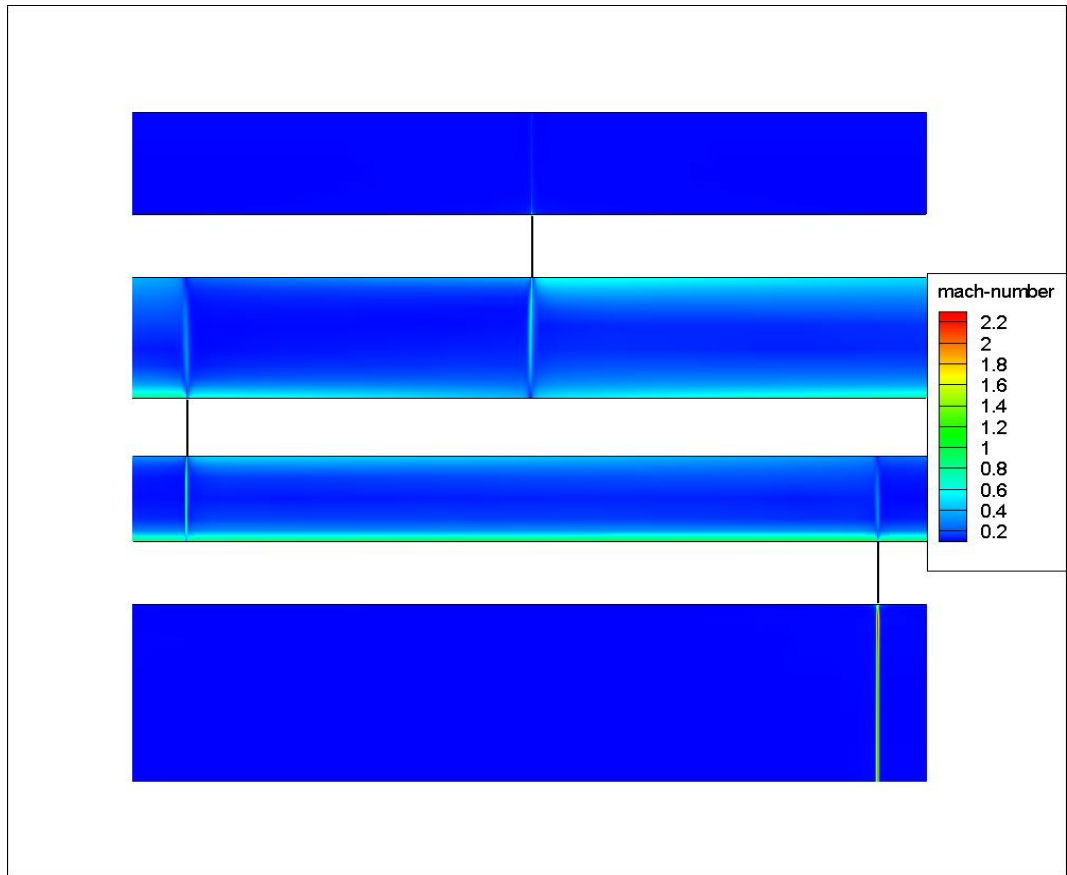
Figure 3.11 Mach contours at maximum combustion chamber pressure (around 1string end gap) (2100 rpm, full load)



(b) Laminar

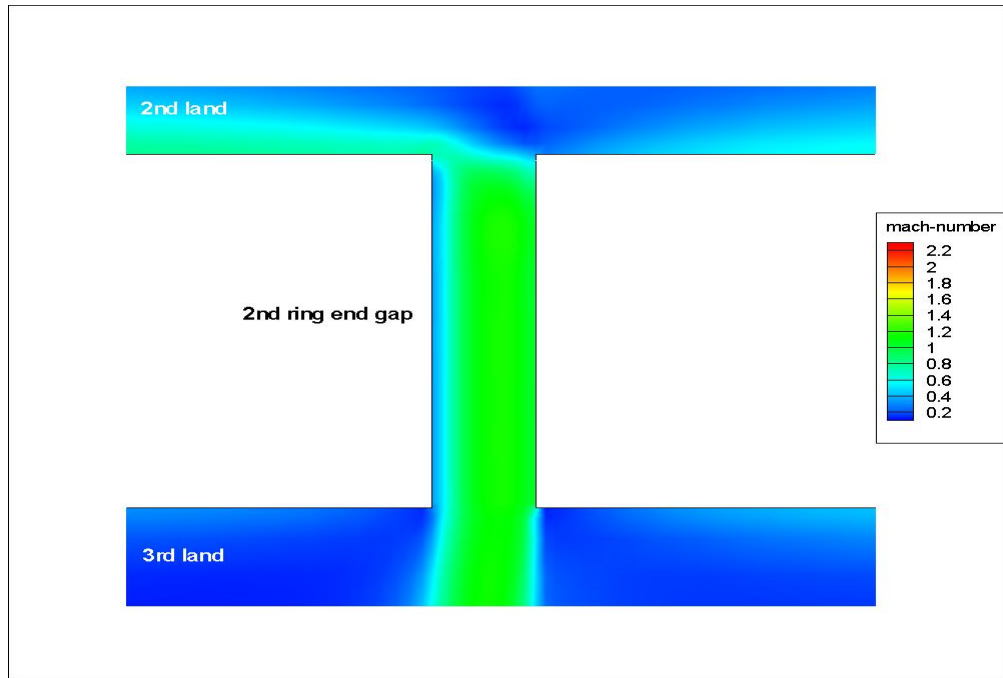
Figure 3.11 Mach contours at maximum combustion chamber pressure
(around 1st ring end gap) (2100 rpm, full load) (Continued)

In Figure 3.11 (a), (b), (c) and (d) Mach contours at maximum 2nd land pressure for full load 2100 rpm engine speed condition are given. In the 2nd land maximum pressure condition, 2nd land pressure is nearly same to the combustion chamber pressure. Gas flows from 2nd land to the 3rd land through the second ring end gap. Therefore 120° angle flow circulation gets weaker in the 2nd land. Detailed Mach contour around second ring end gap can be seen on Figure 3.11 (b). Because of weak 120° flow circulation in 2nd land, high speed flow occurs on the side of the second ring end gap.

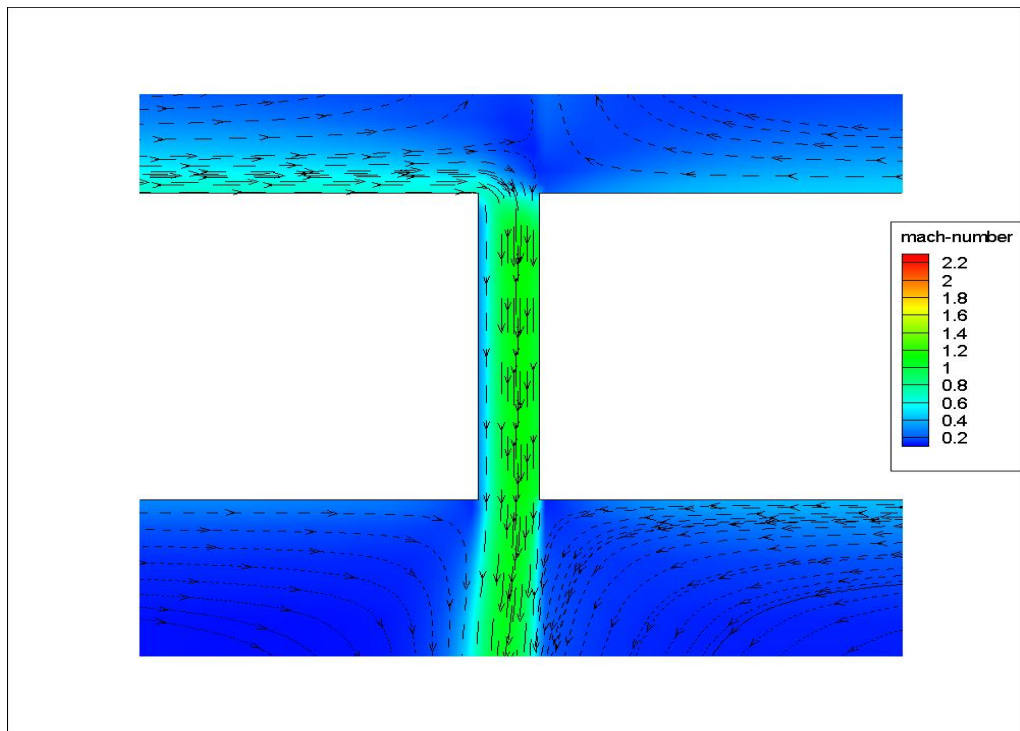


(a) Mach contours (not to scale)

Figure 3.12 Mach contours at maximum 2nd land pressure
(2100 rpm, full load)

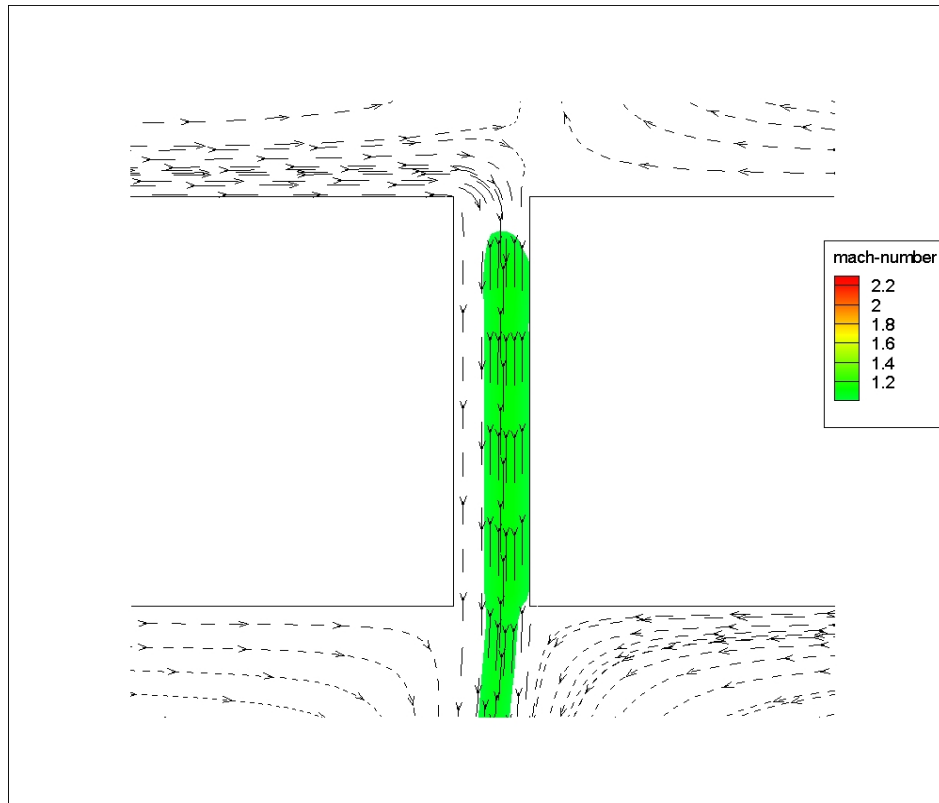


(b) Mach contours (2nd ring end gap)



(c) Streamlines (2nd ring end gap)

Figure 3.12 Mach contours at maximum 2nd land pressure
(2100 rpm, full load) (Continued)



(d) Mach > 1 (2nd ring end gap)

Figure 3.12 Mach contours at maximum 2nd land pressure
(2100 rpm, full load) (Continued)

In Figure 3.13, Mach contours at maximum combustion chamber pressure for full load 2100 rpm engine speed condition are given for the case when all three ring end gaps are aligned. If ring end gaps are aligned, blowby values increase about 8%. Because of increased blowby values, 2nd and 3rd land maximum pressures are lower than the baseline case.

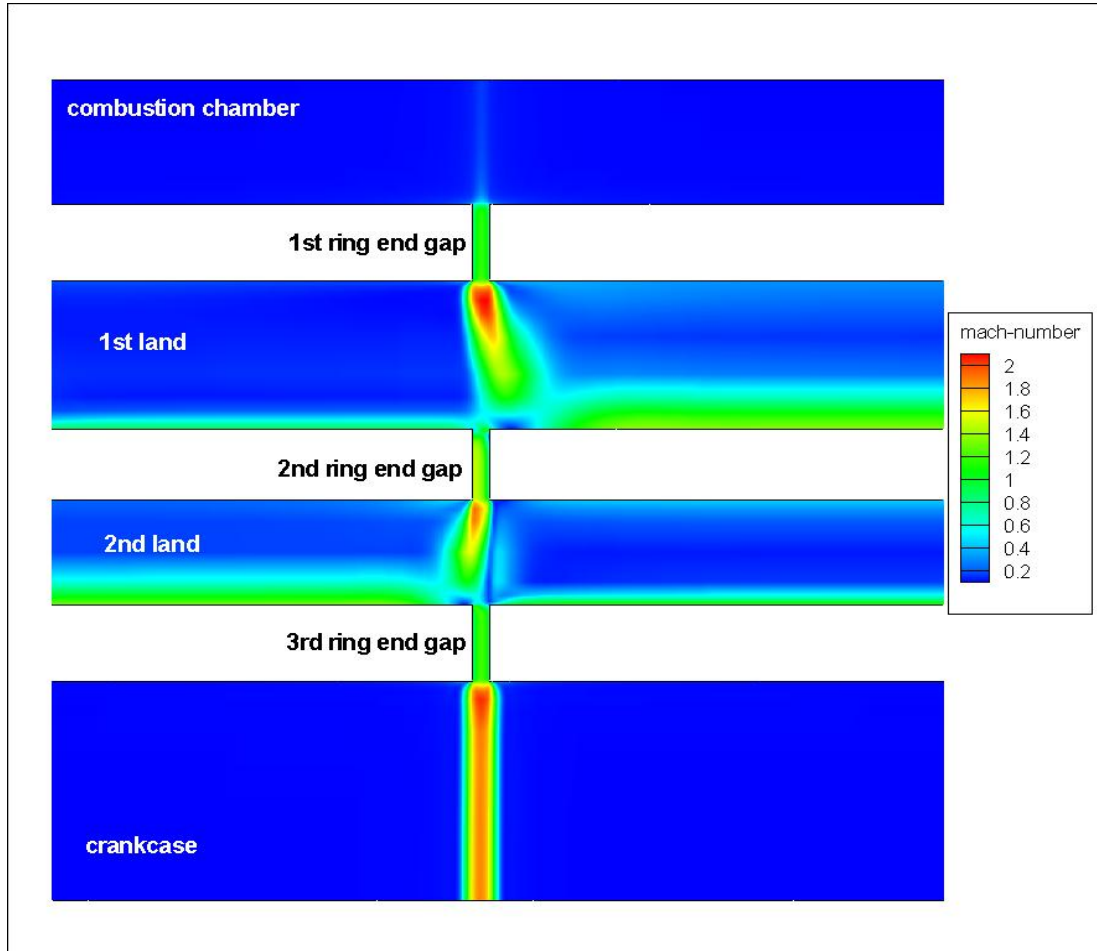


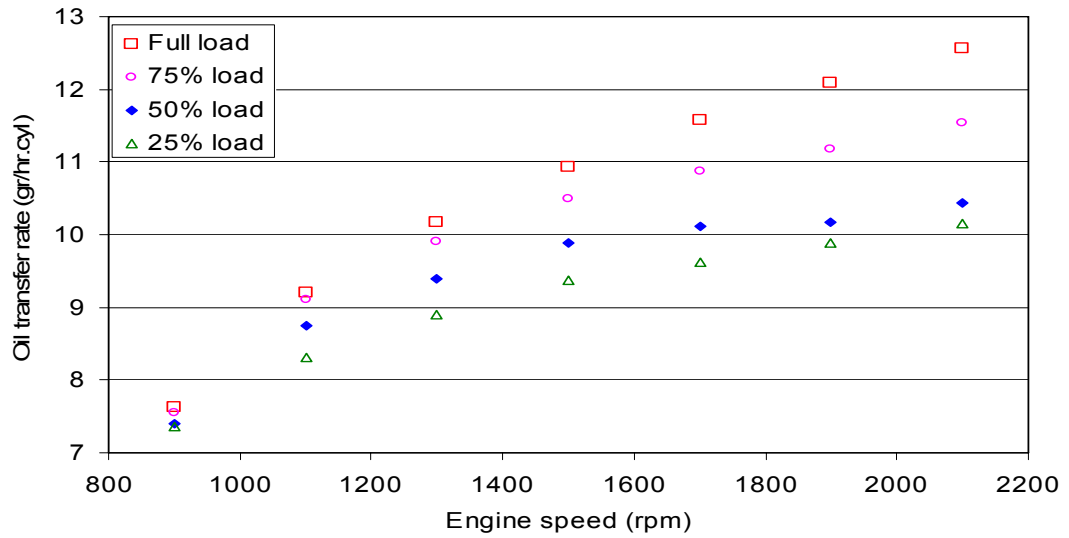
Figure 3.13 Mach contours at maximum 1st land pressure (all ring end gaps are aligned) (2100 rpm, full load) (not to scale)

3.2 Oil Flow Analysis Results

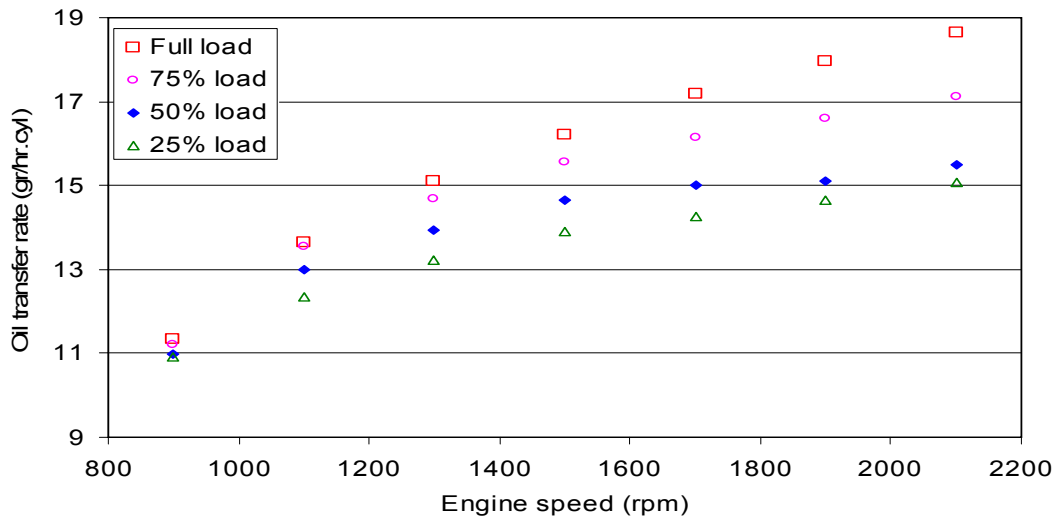
After completing the gas flow analysis, oil consumption at different film thicknesses is analyzed with the help of data obtained from the gas flow analysis.

In Figure 3.12 (a), (b) and (c), oil mass transfer rate at different engine loads and different engine speeds are presented. In actual conditions, oil film thickness is not constant from combustion chamber to the crank case. But in this study, oil film thickness is taken as constant throughout the piston. In addition to this, oil is only entrained from the ring end gaps. In Figure 3.12 (a), (b) and (c) 1, 3 and 5 micron oil film thickness results are given, respectively. At lower engine speed conditions,

engine loads has not an important effect on the oil consumption. But in the higher engine speeds, change of engine load affects oil consumption more. Engine speed also affects oil transfer to the combustion chamber. In higher engine speeds, oil backflow is always more than oil backflow in lower engine speeds.

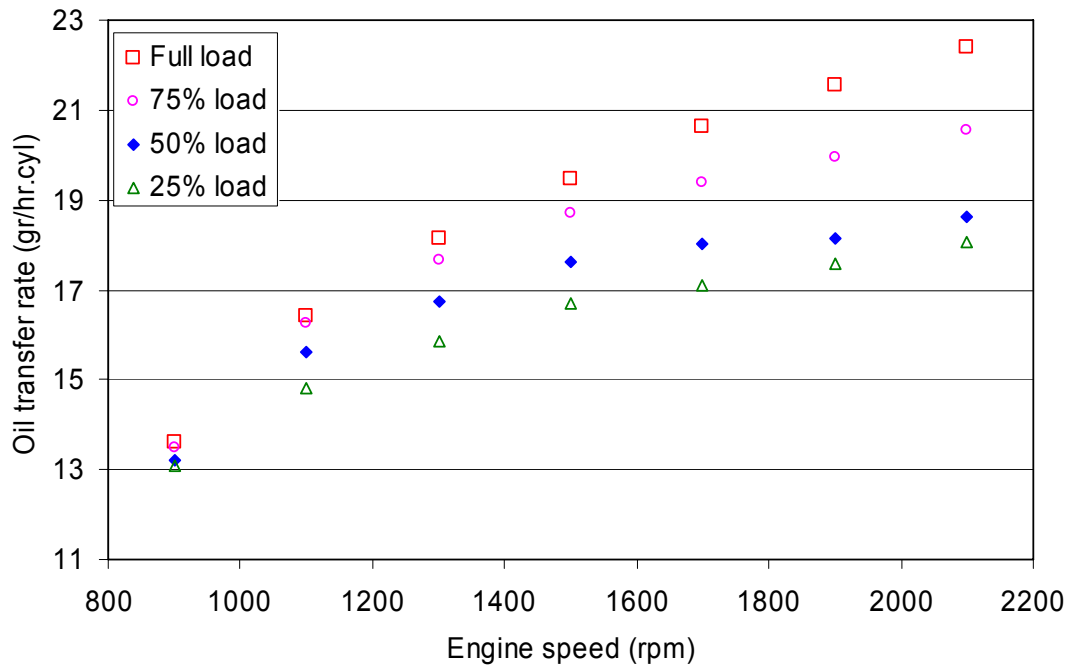


(a) 1 micron oil film thickness



(b) 3 micron oil film thickness

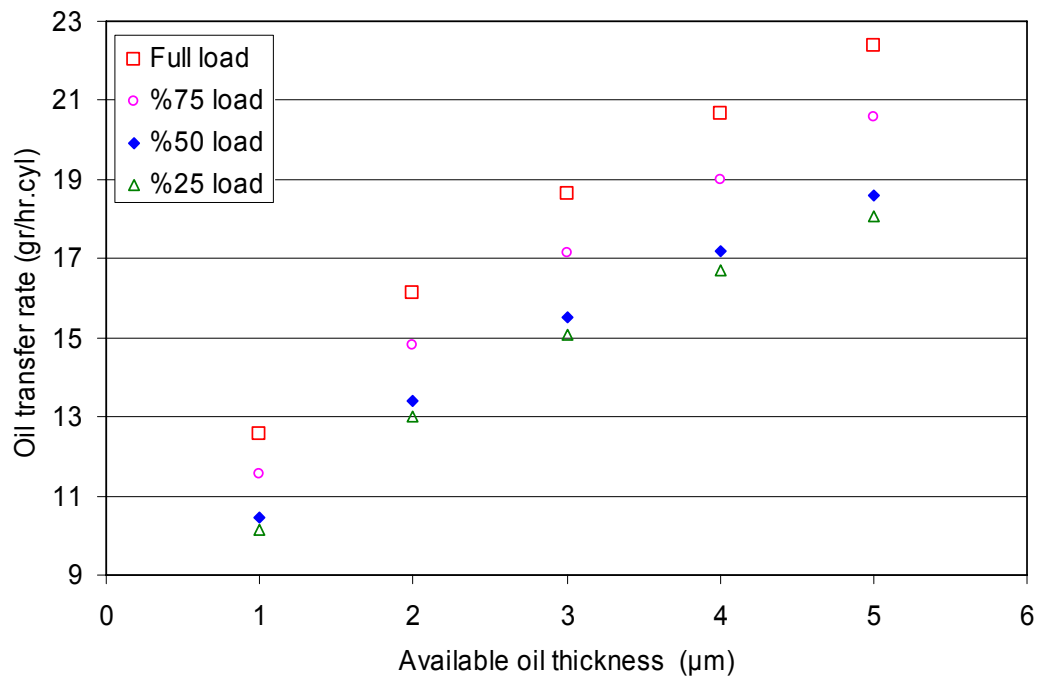
Figure 3.14 Backflow oil transfer to combustion chamber at different oil film thickness



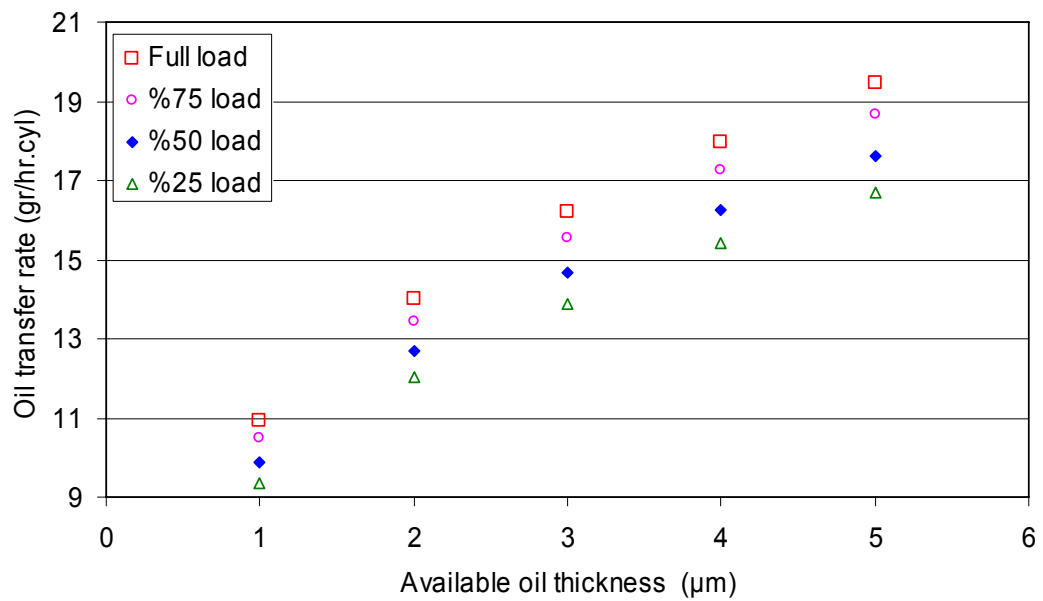
(c) 5 micron oil film thickness

Figure 3.14 Backflow oil transfer to combustion chamber at different oil film thickness (Continued)

In Figure 3.13 (a), (b) and (c), relation between oil consumption, oil film thickness and engine loads are presented. Oil transfer rate to the combustion chamber is always proportional to oil film thickness in the same loading condition. Besides, oil consumption is increased with increasing engine loads in 1500 and 2100 rpm engine speeds, but in 900 rpm engine speed, loading condition has no effect on oil consumption.

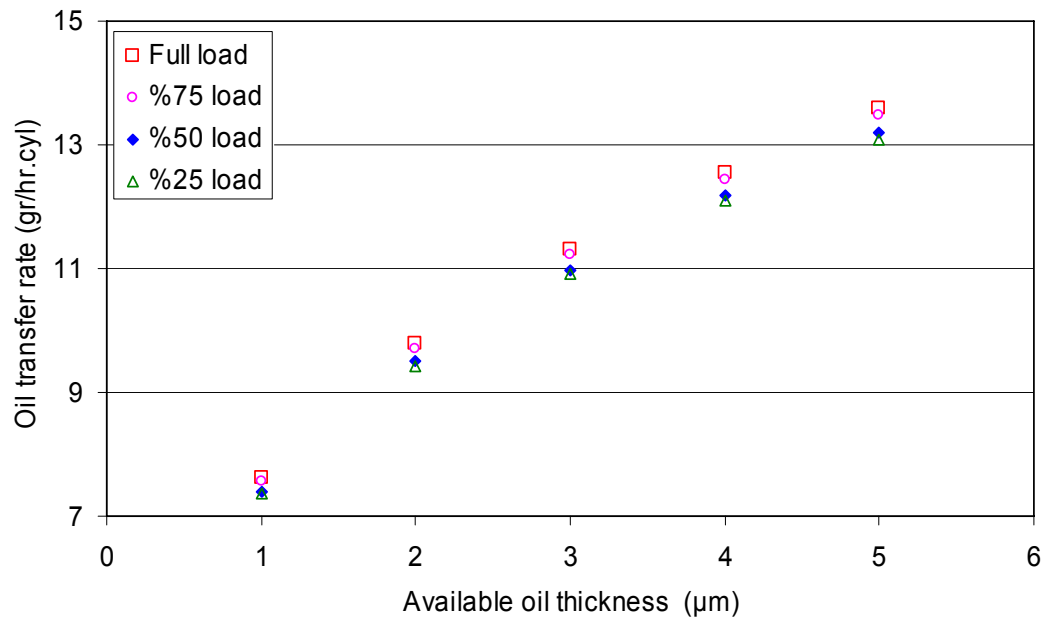


(a) 2100 rpm



(b) 1500 rpm

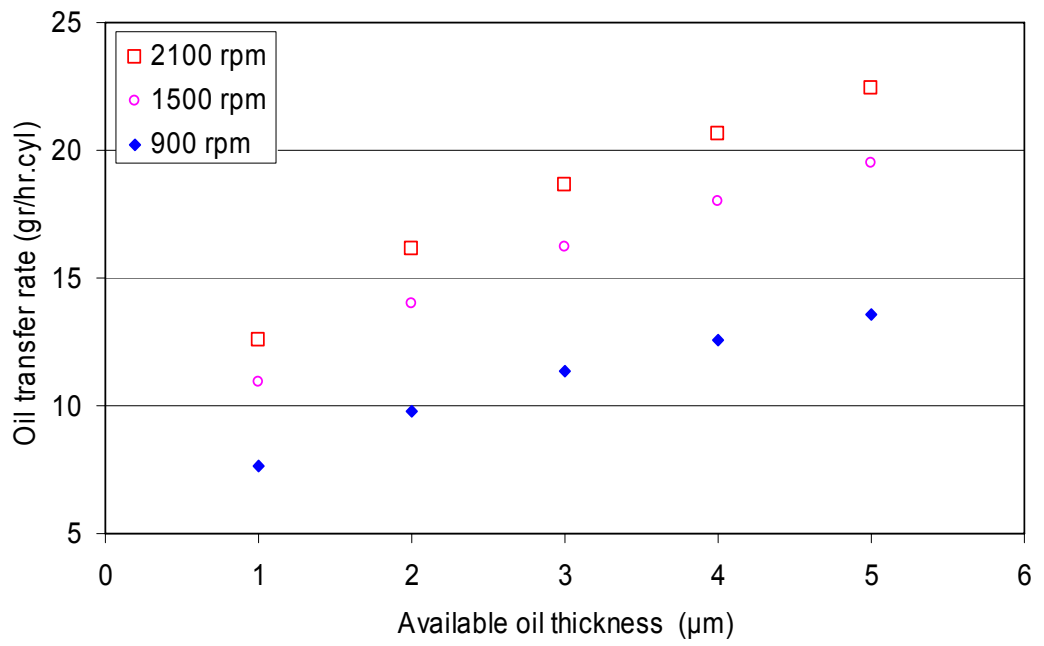
Figure 3.15 Backflow oil transfer to combustion chamber at different engine speeds and loads



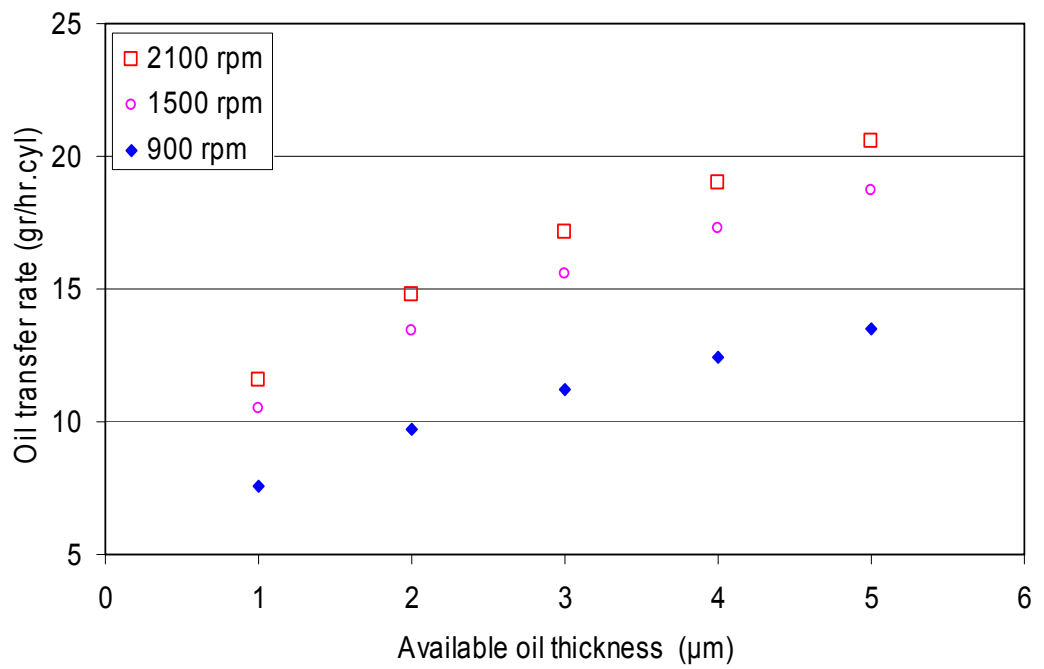
(c) 900 rpm

Figure 3.15 Backflow oil transfer to combustion chamber at different engine speeds and loads (Continued)

Oil backflow relation with engine speeds and oil film thickness can be seen in Figure 3.14 (a), (b), (c) and (d). Similar to the engine loading effect, in higher engine speeds oil transfer rate is more than oil transfer in lower engine speeds. In addition, oil backflow is proportional to oil film thickness in the same engine operation conditions.

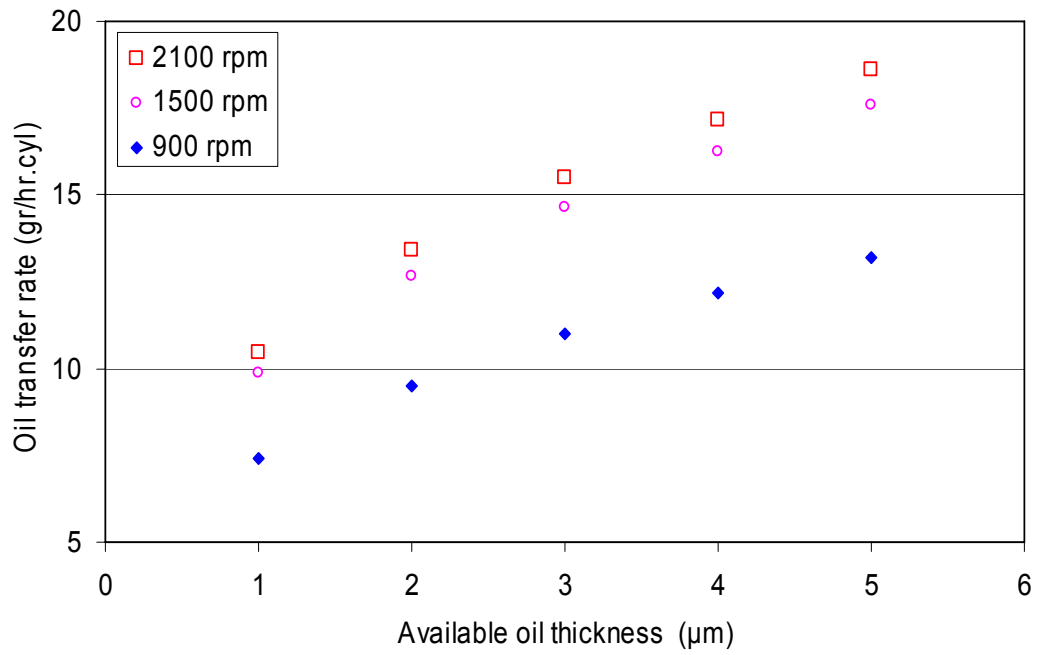


(a) Full load

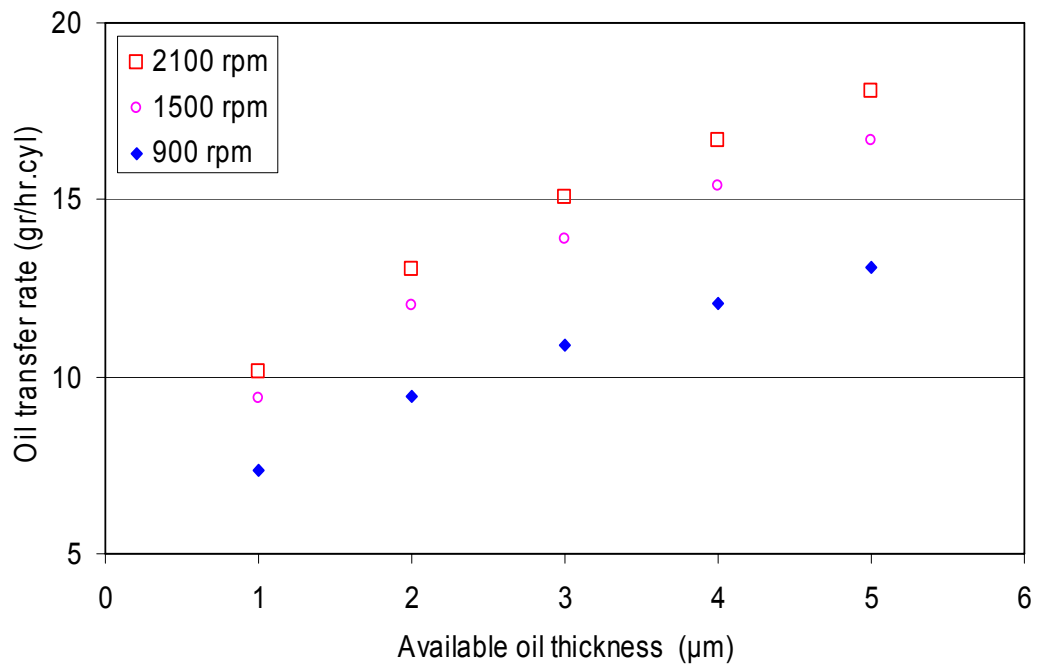


(b) 75% load

Figure 3.16 Backflow oil transfer to combustion chamber at different engine loads and speeds



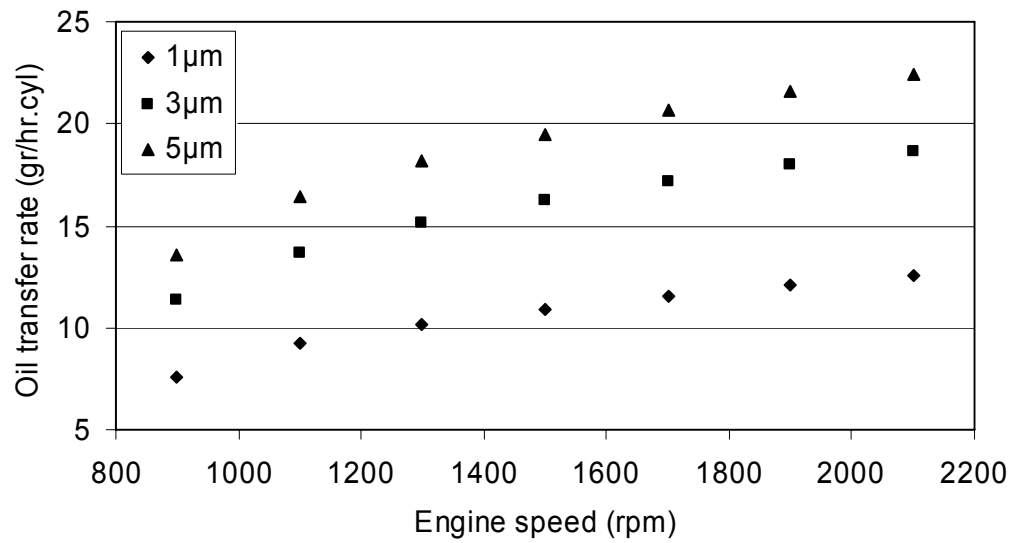
(c) 50% load



(d) 25% load

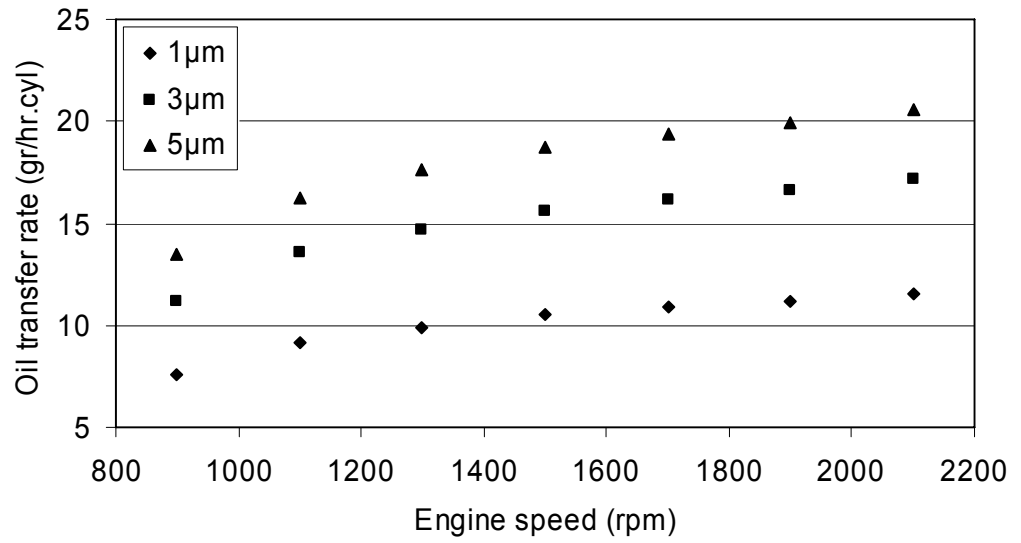
Figure 3.16 Backflow oil transfer to combustion chamber at different engine loads and speeds (Continued)

In Figures 3.15 (a), (b) and (c), backflow of oil at different engine loads and oil film thicknesses can be seen. According to Equation (2.18), entrainment rate is directly related with Reynolds number and entrainment fraction. Entrainment fraction is also a function of Reynolds number. Reynolds number is affected from film superficial velocity which is a function of oil film thickness. Therefore oil transfer rate is directly related to oil film thickness.

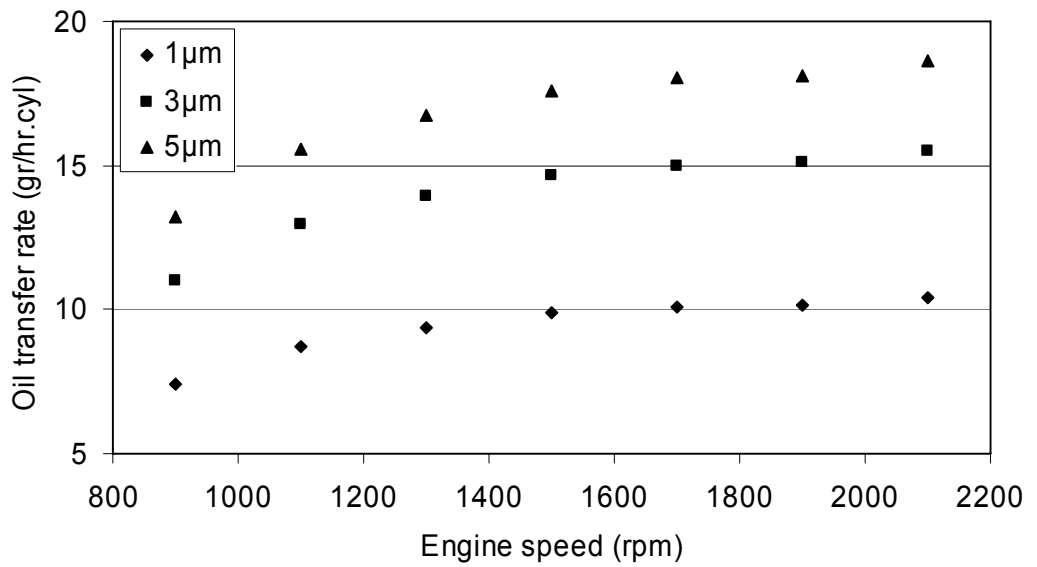


(a) 100% load

Figure 3.17 Backflow oil transfer to combustion chamber at different engine loads and oil thicknesses

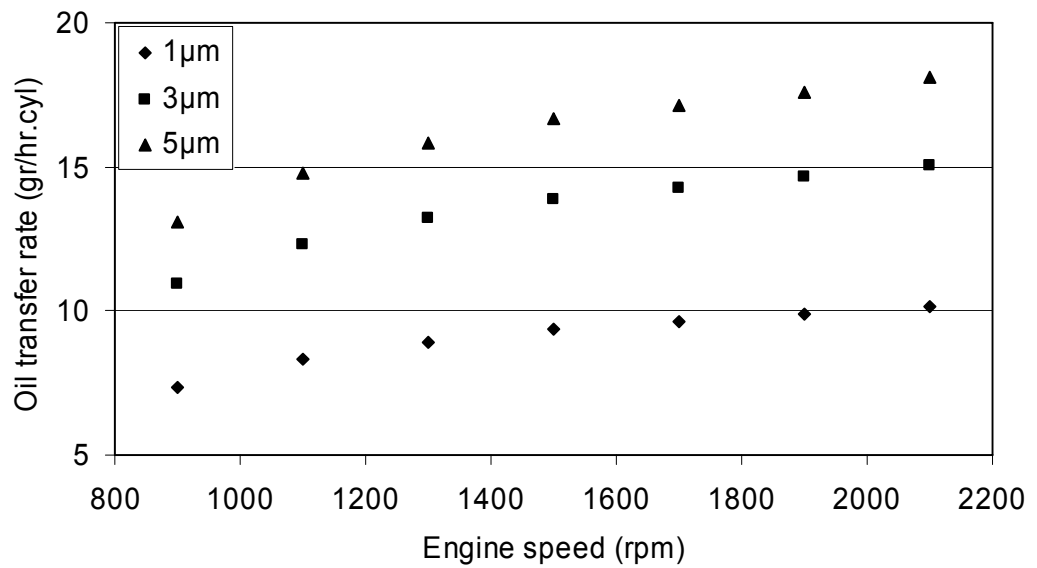


(b) 75% load



(c) 50% load

Figure 3.17 Backflow oil transfer to combustion chamber at different engine loads and oil thicknesses (Continued)



(d) 25% load

Figure 3.17 Backflow oil transfer to combustion chamber at different engine loads and oil thicknesses (Continued)

Similar to oil film thickness effect, oil viscosity affects Reynolds number and entrainment rate directly. In the higher viscosities of oil, air flow cannot easily tear oil from the surface. But in the lower viscosities of oil, air flow can easily tear oil from the surface. Therefore oil transfer rates in higher viscosities are less and in lower viscosities are more than the base case (Figure 3.16).

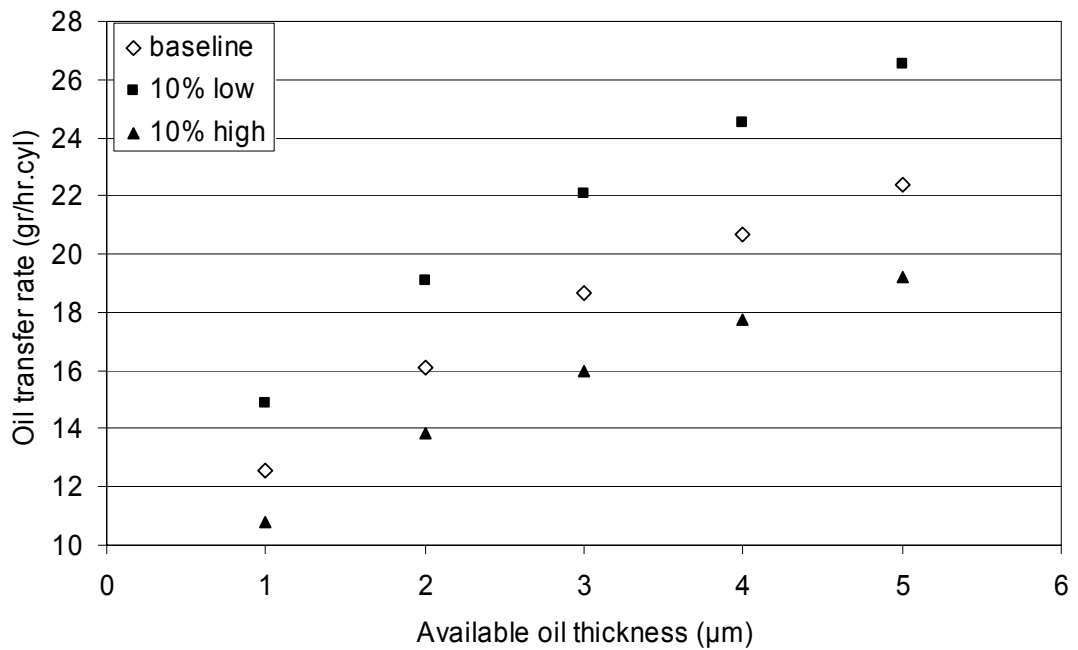


Figure 3.18 Backflow oil transfer to combustion chamber for different oil viscosities at 2100 rpm full load

In Figure 3.17, oil transfer rates at 10% smaller and 10% larger top ring end gaps than base case are shown. At 10% larger top ring end gap, oil entrainment surface is larger and at 10% smaller top ring end gap, oil entrainment surface is also smaller than base case. Therefore oil transfer rates are less at 10% smaller top ring end gap and more at 10% larger ring end gap.

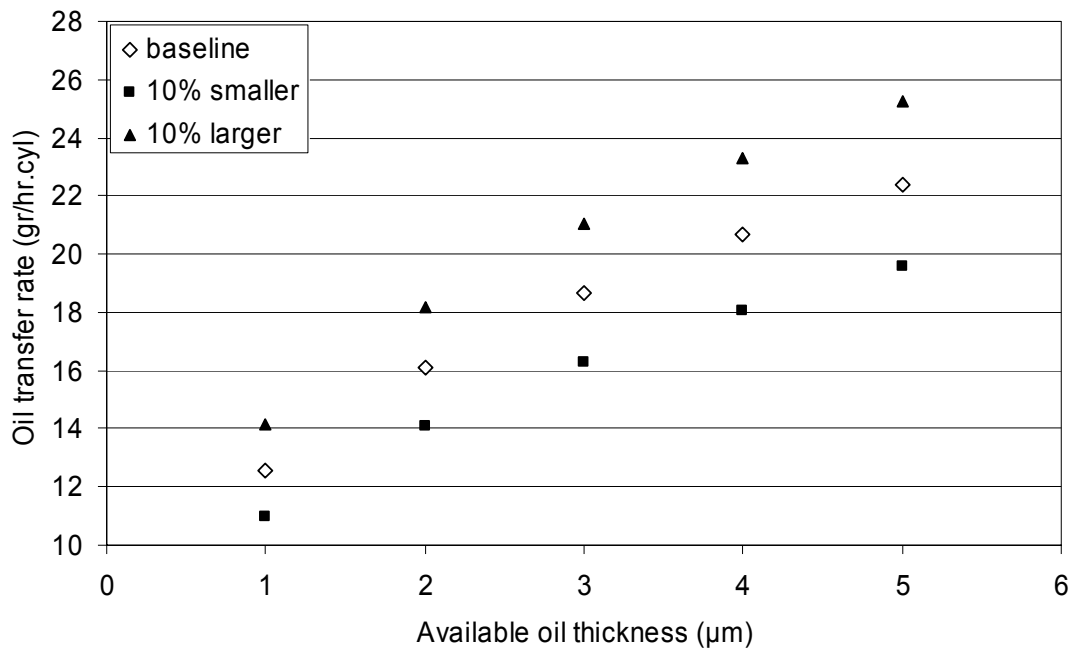


Figure 3.19 Backflow oil transfer to combustion chamber for different oil viscosities at 2100 rpm full load

In Figure 3.18, oil consumption at different physical properties and dimensions are given. In the last column of Figure 3.18, oil consumption results taken from literature are given. Wong and Hoult [4] used 75mm bore diameter and 70mm stroke small diesel engine to make experiments and used SAE 15W-40 oil as lubricant. Tritium was used to measure oil consumption. At 2000 rpm engine operation condition, exhaust of the engine contained 1.2g/h.cyl. Miyachika et al. [16] used sulfur as a tracer to determine oil consumption. Oil consumption was measured about 7.0g/hr.cyl at 2000 rpm engine operation condition. Lizumi and Koyama [17] used S-trace method to determine oil consumption. They worked on 6-cylinder, 140mm stroke, and 135mm bore diameter diesel engine. At 1840rpm and 80% load condition, average oil consumption from six cylinders of the engine is about 6.5g/hr.cyl. All oil consumption results taken from literature are experimental results. Current study analysis results are comparable with the experimental literature results.

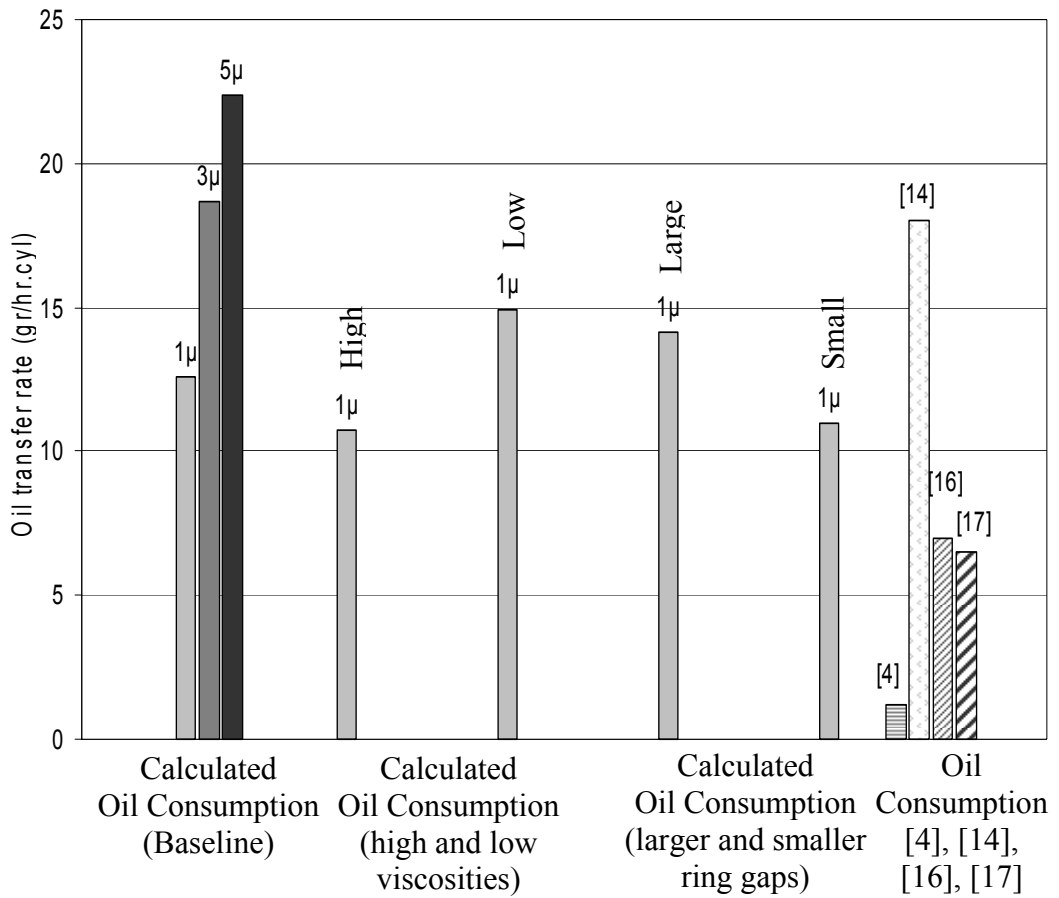


Figure 3.20 Oil consumption for different physical properties and dimensions

CHAPTER 4

CONCLUSIONS

In the current study, a 2D model of the volume between the piston and cylinder is constructed and gas flow through this volume is analyzed. 2nd and 3rd land pressure changes during operation of the engine are determined. 1st, 2nd and 3rd ring end gap mass flow rates and gas velocities are obtained. These land pressure and velocity data are calculated at different top ring end gaps, different engine speeds and different engine loading conditions. With the help of gas flow analysis results, oil transfer rate to the combustion chamber is calculated at different engine speeds and loading conditions. Oil thickness effect is also examined in the oil backflow analysis. According to gas flow and oil flow analysis results following conclusions are made,

- 1) 2nd and 3rd land pressure variations and maximum pressure values are similar to the compared references.
- 2) Gas velocities in the ring end gap or after the ring end gap can be supersonic during a certain part of the engine cycle.
- 3) Calculated gas blowby results are comparable with the literature, even though ring dynamics is not taken into consideration.

- 4) Oil consumption values are affected by the engine speeds, engine loading condition, ring end gap, oil film thickness and oil viscosity.
- 5) Oil consumption results are similar to the experimental literature results.

In this study, gas flow between piston and cylinder is modeled as 2D. Oil consumption rates are calculated by using conservation of mass and entrainment rate correlation. However, the used entrainment rate correlation is not developed for air-oil, high pressure ratio and high speed flows. As a future work, gas flow can be modeled as 3D and ring dynamics can be included. Besides, air-water entrainment correlation should be verified for high pressure ratio, air-oil two-phase flow with the help of experimental entrainment data.

REFERENCES

- [1] Hanaoka, M., Ise, A., Nagasaka, N., Osawa, H. Arakawa, Y. and Obata, T., 1979, “New Method for Measurement of Engine Oil Consumption (S-Trace Method)”, SAE Paper No: 790936.

- [2] Wahiduzzaman, S., Keribar, R., Dursunkaya, Z. and Kelley, F.A., 1992, “A Model for Evaporative Consumption of Lubricating Oil in Reciprocating Engines”, SAE Paper No: 922202.

- [3] Nakashima, K., Ishihara, s., Urano, K. and Murata, K., 1996, “Lubricating Oil Flow into the Combustion Chamber and its Reduction Method in an Automobile Gasoline Engine”, SAE Paper No: 962034.

- [4] Wong, V.W. and Hoult, D.P., 1991, “Experimental Survey of Lubricant-Film Characteristics and Oil Consumption in a Small Diesel Engine”, SAE Paper No: 91741.

- [5] Woodmansee, D.E. and Hanratty, T.J., 1969, “Mechanism for the Removal of Droplets from a Liquid Surface by a Parallel Air Flow”, Chemical Engineering Science, Vol. 24, pp. 299-307.

- [6] Hugmark, G.A., 1973, “Film Thickness, Entrainment, and Pressure Drop in Upward Annular Dispersed Flow”, AIChE Journal, Vol. 19, No. 5, pp. 1062-1065.

- [7] Ishii, M. and Grolmes, M.A., 1975, "Inception Criteria for Droplet Entrainment In Two-Phase Concurrent Film Flow", *AIChE Journal*, Vol. 21, No. 2, pp. 308-318.
- [8] Ishii, M. and Mishima, K., 1989, "Droplet Entrainment Correlation In Annular Two-Phase Flow", *Int. J. Heat Mass Transfer*, Vol. 32, No. 10, pp. 1853-1846.
- [9] Kataoka, I., Ishii, M. and Nakayama, A., 2000, "Entrainment and Deposition Rates In Annular Two-Phase Flow", *Int. J. Heat Mass Transfer*, Vol. 43, pp. 1573-1589.
- [10] Okawa, T., Kitahara, T., Yoshida, K., Matsumoto, T. and Kataoka, I., 2002, "New Entrainment Rate Correlation In Annular Two-Phase Flow Applicable to Wide Range of Flow Condition", *Int. J. Heat Mass Transfer*, Vol. 45, pp. 87-98.
- [11] Okawa, T. and Kataoka, I., 2005, "Correlations for the Mass Transfer Rate of Droplets In Vertical Upward Annular Flow", *Int. J. Heat Mass Transfer*, Vol. 48, pp. 4766-4778.
- [12] Sawant, P., Ishii, M. and Ori, M., 2008, "Droplet Entrainment Correlation In Vertical Upward Co-Current Annular Two-Phase Flow", *Nuclear Engineering and Design*, Vol. 238, pp. 1342-1352.
- [13] İçöz, T., 2001, "Experimental Investigation of Oil Accumulation in the Inter Ring Volumes in Internal Combustion Engines", M.S. Thesis, Department of Mechanical Engineering, METU.
- [14] Karkaç, A., 2002, "Backflow Oil Transfer in Internal Combustion Engines", M.S. Thesis, Department of Mechanical Engineering, METU.

- [15] Keribar, R., Dursunkaya, Z. and Flemming, M.F., 1991, "An Integrated Model of Ring Pack Performance", Transactions of the ASME, Vol. 113, pp. 382-389.
- [16] Miyachika, M., Hirota, T. and Kashiya, K., 1984, "A Consideration on Piston Second Land Pressure and Oil Consumption of Internal Combustion Engine", SAE Paper No: 840099.
- [17] Lizumi, S. and Koyama, T., 1986, "Measurement of Oil Consumption of Diesel Engine by S-Trace Method", SAE Paper No: 86545.
- [18] FLUENT[®], <http://www.fluent.com/software/fluent/index.htm>, 09/09/2009
- [19] GAMBIT[®], <http://www.fluent.com/software/gambit/index.htm>, 09/09/2009
- [20] Schlichting, H., 1979, "Boundary Layer Theory", McGraw-Hill, New York, pp. 502-531.

APPENDIX A

OIL GAS INTERFACE VELOCITY CALCULATION

Shearing stresses at the interface of oil-gas have to be equal and they are defined as follows

Shear force of oil:

$$\tau_0 = \frac{dP}{dx} \frac{R}{2} = \frac{dP}{dx} \frac{h}{2} \quad (\text{A } 1)$$

Shear force of gas:

$$\tau_0 = 0.0225 \rho_{gas} V_{max}^{7/4} \left(\frac{v_{gas}}{h} \right)^{1/4} \quad (\text{A } 2)$$

They have to be equal at the oil gas interface.

$$\frac{dP}{dx} \frac{h}{2} = 0.0225 \rho_{gas} V_{max}^{7/4} \left(\frac{v_{gas}}{h} \right)^{1/4} \quad (\text{A } 3)$$

rearranging Equation (A.3)

$$\frac{dP}{dx} = \frac{0.045}{h} \rho_{gas} V_{max}^{7/4} \left(\frac{v_{gas}}{h} \right)^{1/4} \quad (A 4)$$

$$\frac{dP}{dx} = 0.045 \frac{\rho_{gas} V_{max}^2}{h} \left(\frac{v_{gas}}{h V_{max}} \right)^{1/4} \quad (A 5)$$

Reynolds number can be defined as

$$Re = \frac{h V_{max}}{v_{gas}} \quad (A 6)$$

then Equation (A.5) becomes

$$\frac{dP}{dx} = \frac{0.045}{Re^{1/4}} \left(\frac{\rho_{gas} V_{max}^2}{h} \right) \quad (A 7)$$

Oil velocity profile is defined in Equation (2.12). Combining equations (2.12) and (A.7)

$$V_{oil} = \frac{1}{2\mu_{oil}} \left(\frac{0.045 \rho_{gas} V_{max}^2}{h Re^{1/4}} \right) y^{*2} + b_1 y^* \quad (A 8)$$

Multiplying with V_{max}

$$\frac{V_{oil}}{V_{max}} = \left[\frac{1}{2\mu_{oil}} \frac{0.045 \rho_{gas} V_{max}}{Re^{1/4} h} \right] y^{*2} + \frac{b_1}{V_{max}} y^* \quad (A 9)$$

Multiplying the first term of Equation (A.9) with h^2/h^2 . Then Equation (A.9) becomes

$$\frac{V_{oil}}{V_{max}} = \frac{0.045}{2 Re^{1/4}} \frac{\rho_{gas} V_{max} h}{\mu_{oil}} \frac{y^{*2}}{h^2} + \frac{b_1}{V_{max}} y^* \quad (A 10)$$

To simplify equations, A is defined as

$$A = \frac{\rho_{gas} V_{max} h}{\mu_{oil}} \quad (A 11)$$

then Equation (A.10) becomes

$$\frac{V_{oil}}{V_{max}} = \frac{0.0225 A}{Re^{1/4}} \frac{y^{*2}}{h^2} + \frac{b_1}{V_{max}} y^* \quad (A 12)$$

Multiplying the first term of Equation (A.12) with t^2/t^2 , and the second term of with t/t , then Equation (A.13) is obtained.

$$\frac{V_{oil}}{V_{max}} = 0.0225 \frac{A}{Re^{1/4}} \frac{t^2}{h^2} \frac{y^{*2}}{t^2} + \frac{b_1 t}{V_{max}} \frac{y^*}{t} \quad (A 13)$$

To simplify Equation (A.13), C is defined as

$$C = \frac{b_1 t}{V_{max}} \quad (A 14)$$

Then Equation (A.13) can be written as,

$$\frac{V_{oil}}{V_{max}} = 0.0225 \frac{A}{Re^{1/4}} \frac{t^2}{h^2} \frac{y^{*2}}{t^2} + C \frac{y^*}{t} \quad (A 15)$$

To obtain oil gas interface velocity, continuity property of velocity and shear stress at interface is used and the following boundary conditions are used.

Continuity of longitudinal velocity,

$$\frac{y^*}{t} = 1, y = 0; \quad V_{oil} = V_{gas} \quad (A 16)$$

Continuity of shear stress,

$$\frac{y^*}{t} = 1, y = 0; \quad \tau_{oil} = \tau_{gas} \quad (A 17)$$

Shear stress for oil and gas,

$$\tau_{oil} = \mu_{oil} \frac{\partial V_{oil}}{\partial y^*} \quad (\text{A } 18)$$

$$\tau_{gas} = \mu_{gas} \frac{\partial V_{gas}}{\partial y^*} \quad (\text{A } 19)$$

Using the interface conditions, Equation (A.15) and Equation (2.11) can be written as

$$\frac{V_{oil}}{V_{max}} = 0.0225 \frac{A}{\text{Re}^{1/4}} \frac{t^2}{h^2} (1)^2 + C(1) \quad (\text{A.20})$$

and

$$\frac{V_{gas}}{V_{max}} = \left(\frac{0 + \delta}{h} \right)^{1/6} \quad (\text{A.21})$$

To simplify Equation (A.20), D is defined as

$$D = 0.0225 \frac{A}{\text{Re}^{1/4}} \frac{t^2}{h^2} \quad (\text{A.22})$$

Combining velocity Equations (A.20) and (A.21) at oil-gas interface

$$D + C = \left(\frac{\delta}{h} \right)^{1/6} \quad (\text{A.23})$$

Rearranging

$$C = \left(\frac{\delta}{h} \right)^{1/6} - D \quad (\text{A.24})$$

Using the interface conditions in the shear stress equations give

$$\tau_{oil} = \mu_{oil} \left[\left(0.0225 \frac{A}{\text{Re}^{1/4}} \frac{t^2}{h^2} \frac{2y^*}{t^2} + C \frac{1}{t} \right) V_{\max} \right] \text{ at } \frac{y^*}{t} = 1 \quad (\text{A.25})$$

$$\tau_{oil} = \mu_{oil} \left[\left(0.0225 \frac{A}{\text{Re}^{1/4}} \frac{t^2}{h^2} \frac{2}{t} + C \frac{1}{t} \right) V_{\max} \right] \quad (\text{A.26})$$

and

$$\tau_{gas} = \mu_{gas} \left[\frac{1}{6h} \left(\frac{y + \delta}{h} \right)^{-5/6} \right] V_{\max} \text{ at } y = 0 \quad (\text{A.27})$$

$$\tau_{gas} = \mu_{gas} \left[\frac{1}{6h} \left(\frac{\delta}{h} \right)^{-5/6} \right] V_{\max} \quad (\text{A.28})$$

At the oil-gas interface shear stress of oil has to be equal to shear stress of gas.

$$\tau_{oil} = \tau_{gas} \quad (\text{A.29})$$

Combining Equations (A.26) and (A.28)

$$\mu_{oil} \left[\left(0.0225 \frac{A}{\text{Re}^{1/4}} \frac{t^2}{h^2} \frac{2}{t} + C \frac{1}{t} \right) V_{\max} \right] = \mu_{gas} \left[\frac{1}{6h} \left(\frac{\delta}{h} \right)^{-5/6} \right] V_{\max} \quad (\text{A.30})$$

$$\mu_{oil} \left(0.0225 \frac{A}{\text{Re}^{1/4}} \frac{t^2}{h^2} \frac{2}{t} + C \frac{1}{t} \right) = \mu_{gas} \left[\frac{1}{6h} \left(\frac{\delta}{h} \right)^{-5/6} \right] \quad (\text{A.31})$$

To simplify Equation (A.31), μ_{rel} is defined as

$$\mu_{rel} = \frac{\mu_{gas}}{\mu_{oil}} \quad (\text{A.32})$$

And by using D, Equation (A.31) becomes

$$\frac{2D}{t} + \frac{C}{t} = \mu_{rel} \frac{1}{6h} \left(\frac{\delta}{h} \right)^{-5/6} \quad (\text{A.33})$$

Rearranging

$$C = \mu_{rel} \frac{t}{6h} \left(\frac{\delta}{h} \right)^{-5/6} - 2D \quad (\text{A.34})$$

Combining Equations (A.24) and (A.34)

$$\mu_{rel} \frac{t}{6h} \left(\frac{\delta}{h} \right)^{-5/6} - 2D = \left(\frac{\delta}{h} \right)^{1/6} - D \quad (\text{A.35})$$

To simplify equations use

$$\alpha = \frac{\delta}{h} \quad (\text{A.36})$$

$$E = \frac{t\mu_{rel}}{6h} \quad (\text{A.37})$$

Then Equation (A.35) can be written as

$$E\alpha^{-5/6} - 2D = \alpha^{1/6} - D \quad (\text{A.38})$$

Rearrange

$$\alpha^{1/6} + D\alpha^{5/6} - E = 0 \quad (\text{A.39})$$

Root of Equation (A.39) can be calculated using Secant method at every time step and result is substituted in the Equation (2.11) to calculate the interface velocity.